Potential desiccation cracks on Mars: A synthesis from modeling, analogue-field studies, and global observations

M.R. El-Maarry [a,*], W. Watters [b], N.K. McKeown [c], J. Carter [d], E. Noe Dobrea [e,f], J.L. Bishop [g], A. Pommerol [a], N. Thomas [a]

[a] Physikalisches Institut, Bern Univeristät, Sidlerstrasse, 5, 3012 Berne, Switzerland
[b] Whitin Observatory, Department of Astronomy, Wellesley College, Wellesley, MA, 02481, USA
[c] Department of Physical Sciences, MacEwan University, Edmonton, Alberta, Canada
[d] Institut d'Astrophysique Spatiale, Paris-Sud University, Orsay, France
[e] Planetary Science Institute, Tucson, AZ, 85719, USA
[f] NASA Ames Research Center, Mountain View, CA, 94035, USA
[g] SETI Institute, Mountain View, CA 94043, USA

ARTICLE INFO

ABSTRACT

Potential desiccation polygons (PDPs) are polygonal surface patterns that are a common feature in Noachian-to-Hesperian-aged phyllosilicate- and chloride-bearing terrains and have been observed with size scales that range from cm-wide (by current rovers) to 10s of meters-wide. The global distribution of PDPs shows that they share certain traits in terms of morphology and geologic setting that can aid identification and distinction from fracturing patterns caused by other processes. They are mostly associated with sedimentary deposits that display spectral evidence for the presence of Fe/Mg smectites, Al-rich smectites or less commonly kaolinites, carbonates, and sulfates. In addition, PDPs may indicate paleolacustrine environments, which are of high interest for planetary exploration, and their presence implies that the fractured units are rich in smectite minerals that may have been deposited in a standing body of water. A collective synthesis with new data, particularly from the HiRISE camera suggests that desiccation cracks may be more common on the surface of Mars than previously thought. A review of terrestrial research on desiccation processes with emphasis on the theoretical background, field studies, and modeling constraints is presented here as well and shown to be consistent with and relevant to certain polygonal patterns on Mars.

1. Introduction

1.1. Polygonal patterns on Mars

Surface polygonal patterns are common on Mars. These patterns attain a range of shapes and variable sizes, which can vary from cm- to km-sized patterns. Historically, most of the surface patterns, in particular those observed at high latitudes (>45°), were classified as periglacial features that evolve through thermal contraction (e.g., Mutch et al., 1976; Lucchitta, 1981; Mellon, 1997; Seibert and Kargel, 2001; Mangold, 2005; Levy et al., 2009; Lefort et al., 2010). Nevertheless, the desiccation mechanism was consistently proposed as an alternative mechanism since the Viking era of exploration (e.g., Mutch et al., 1976). The reason for the frequent

suggestion of these two hypotheses is the morphological similarity between polygonal features created by desiccation and thermal contraction at the size-scales that were initially observed (5–20 m-range) making it difficult to differentiate between them on the basis of remote sensing alone.

With the introduction of orbiting high resolution cameras that had tens of meters-scale of spatial resolution and enough spatial coverage and mission longevity to map the entire surface of Mars, researchers observed a latitudinal dependence in the distribution of patterned ground with a clear preference for high latitudes, which indicated that most of the surface patterns, except for perhaps the tectonically-controlled km-sized polygons in Utopia (e.g., Pechmann, 1980; McGill and Hills, 1992; Moscardelli et al., 2012), form by thermal contraction in a periglacial-like climatic setting. Indeed, the current climate on Mars and a multitude of data that indicate that Mars has been cold for the past ∼3 byr support these conclusions (Fairén, 2010 and references therein).

Furthermore, numerical models that take into account the daily and seasonal temperature variations, the presence of near-surface ice, and surface albedo and thermal inertia of frozen soils (e.g., Mellon, 1997; Fisher, 2005; Mellon et al., 2008) have yielded accurate predictions of the expected size-scales of thermal-contraction polygons (TCPs) on Mars (5–20 m in size). These estimates have since been validated by other measurements such as the detection of near-surface ice (within the first meter of the surface) at high latitudes by the Gamma Ray Spectrometer (Boynton et al., 2007) and in-situ analyses made by the Phoenix lander (Smith et al., 2009; Mellon et al., 2009) in addition to extensive mapping work (e.g., Mangold, 2005; Levy et al., 2009), which has recognized the important role of ice-rich soils in shaping the high latitudes of Mars.

A significant leap in our understanding of surface morphology and active processes on Mars was achieved with the insertion of the Mars Reconnaissance Orbiter (MRO) into orbit in 2007. In particular, the High Resolution Imaging Science Experiment (HiRISE; McEwen et al., 2007) onboard MRO allowed observation of the surface of Mars at unprecedented sub-meter (0.25–0.5 m/pixel) scales. Taking advantage of such spatial resolutions, more surface fracture patterns were observed, particularly in the southern highlands, which differ from the conventional morphology and size-scale of TCPs on Mars. In addition, these features do not show a significant latitudinal dependence but instead a regional preference for sedimentary environments that could have harbored liquid water more than 3 byr ago.

1.2. Early climatic conditions on Mars

The geological record of Mars suggests that it has been cold and dry for most of the last 3 byr, except for regionally localized transient events (see Fairén, 2010 and references therein). However, a significant debate remains regarding the first billion years that followed the planet's formation of a solid crust, which generally corresponds to the Noachian period (Scott and Tanaka, 1986; Hartmann and Neukum, 2001). The Noachian crust records various lines of evidence that suggest that there may have been a more globally active hydrological cycle (Carr, 1996 and references therein), and potentially a warmer climate. This evidence includes the presence of valley networks and associated deltas (e.g., Carr, 1986, 1995; Baker et al., 1991; Gulick, 2001; Fasset and Head, 2008; Di Achille and Hynek, 2010; Hynek et al., 2010), explosive volcanism, which involves the interaction and mixing of magma with near-surface volatiles (e.g., Reimers and Komar, 1979; Blasius and Cutts, 1981; Hynek et al., 2003; Wilson and Head, 2007; Kerber et al., 2012), in addition to the surface mineralogical diversity and wide extent of clay minerals as well as other hydrous phyllosilicates (e.g., Poulet et al., 2005; Bibring et al., 2006; Mustard et al., 2009; Murchie et al., 2009; Ehlmann et al., 2009, 2011; Wray et al., 2009; Carter et al., 2010) and salts such as carbonates (e.g., Ehlmann et al., 2008a, 2008b), sulfates (e.g., Langevin et al., 2005; Mangold et al., 2008; Murchie et al., 2009; Wray et al., 2010, 2011) and chlorides (Osterloo et al., 2008, 2010).

Imaging spectrometers, in particular the "Observatoire pour la Minéralogie, l'Eau, les Glaces et l'Activité" (OMEGA) imaging spectrometer (Bibring et al., 2004), and the Compact Reconnaissance Imaging Spectrometer for Mars (CRISM; Murchie et al., 2007) have identified thousands of sites rich in hydrous minerals, and in particular smectites, which are a special family of phyllosilicate minerals that have a high affinity for water, and generally form in environments that feature liquid water activity. In association with these smectites and other hydrous minerals, many researchers have noted the presence of polygonal crack patterns, which have been more often than not, attributed to desiccation of the once water-saturated smectites (e.g. Ehlmann et al., 2008a, 2008b,

2009; Wray et al., 2010, 2011; Erkeling et al., 2012; Bishop et al., 2013a; McKeown et al., 2013; El-Maarry et al., 2013a). Since the vast majority of phyllosilicate occurrences is confined to Noachian-aged terrains (Bibring et al., 2006; Carter et al., 2013), which formed in a period of debatable climatic conditions, understanding the processes that create polygonally cracked terrains can shed light on the climatic conditions during the time of their formation.

1.3. Structure and organization of the paper

We present here a synthesis of the collective evidence that shows that desiccation cracks are more common on the surface of Mars than previously thought. In Section 2, we initially review the state of terrestrial research that is relevant to our study on desiccation processes, field studies, and modeling constraints. At this point we should point out that throughout this paper, we will be citing many terrestrial studies that describe desiccation in terrestrial "soils" that generally include organic matter and imply some form of biological influence, which is generally different from the description of a "sediment", which is a form of material that is eroded, transported and deposited by physical processes such as wind or water. However, in our description of clay-bearing terrains or deposits on Mars, we may sometimes use the terms "soil" and "sediment" interchangeably since a "soil" is generally regarded in planetary literature as simply any fine-grained material including those sufficiently fine-grained to be mobilized by wind (e.g., Karunatillake et al., 2007, and references therein). In Section 3 we present an inventory of the sites on Mars containing potential desiccation polygons (PDPs) and review their geologic setting. Finally, we discuss possible means of identifying desiccation polygons from other polygonal patterns on Mars, as well as their potential value as lithological and climatic indicators in Section 4.

2. Advances in terrestrial research on desiccation

2.1. The desiccation mechanism

Desiccation is usually achieved through evaporation from the surface, or diffusion processes either through the migration of liquid water due to differences in water potential, or vapor transport due to changes in water vapor pressure. The degree to which a material (soil or sediment) contracts with loss of volatiles (usually liquid water) depends on its capacity for holding these volatiles on a macro scale through having a significant pore or void volume within the solid structure, and on a micro scale through its chemical activity and/or ability to accommodate water molecules within its crystal structure (El-Maarry et al., 2012). Generally, the more clay-rich (grain size <2 μm) the soil or sediment is, the more it will shrink with desiccation. In addition, certain clay minerals, known as smectites, are known for their chemical affinity to swell (sometimes several magnitudes beyond their dry volume) and accommodate considerable amounts of water through formation of water interlayers on a molecular level (Velde, 2010).

If the desiccated materials are not allowed to shrink effectively, stresses (mainly tensile) begin to build-up within the desiccated medium creating a stress zone. The thickness of the stressed zone is affected by many factors such as the desiccation rate, the mineralogy, the soil or sediment's physical properties and the presence/absence of salts, which mainly influences the desiccation rate (e.g., Plummer and Gostin, 1981). The stresses that build-up with desiccation may lead to the formation of tensile cracks in the desiccation medium, which we investigate further in the next section.

2.2. Tensile/contraction cracks

Tensile or contraction cracks develop in different geologic materials such as volcanic flows, mud, permafrost, and even rock surfaces. They occur in response to the build-up of stress in a material by various mechanisms that include tectonic extensional forces, cooling, and desiccation. If the material is not allowed to contract (or strain), stresses may build up until they exceed the material's tensile strength, in which case, fractures develop to relieve the stress. The (preliminary) depth of the fractures depends on the thickness of the stressed zone (Section 2.1). Generally, a tensile crack is not expected to propagate much deeper beyond the stressed zone (Lachenbruch, 1961, 1962). A notable exception occurs in cold brittle conditions if the stressed region is sufficiently thin (~cm's-thick). In this particular case, fractures may propagate 3–15 times the depth of the thermally stressed layer (Maloof et al., 2002). For such thin affected layers (i.e., caused by diurnal variations), both gravitational loading and geothermal gradients are not significant. Variations on a seasonal scale, however, create a thicker meter-scale stressed zone, and fractures in that case do not extend far beyond the stressed layer because of compressive stresses and viscous relaxation, which is associated with a transition to warmer temperatures (El-Maarry et al., 2010).

For a given initial stress distribution, the width of the zone of stress relief (i.e. crack spacing) increases with the depth of the fracture (Lachenbruch, 1961, 1962) as deeper fractures release more strain at the surface, which elastically relieves more stress (Fig. 1). The extent of this dependence varies according to the mechanism under investigation. In the case of TCPs and desiccation polygons, the fracture depth-to-spacing ratio usually varies from 1:3 up to 1:10 with the ratios of 1:3–1:4 being the more common (e.g., Lachenbruch, 1962; Corte and Higashi, 1964; Neal et al., 1968; Parker, 1999). Volcanic columnar joints usually have fracture depths several times deeper than the fracture spacing. This special case arises because the fracture spacing is set in the top layer that has hardened, while the deeper and hotter parts of the flow are still fluid (e.g., Müller, 1998; Toramaru and Matsumoto, 2004; Goehring, 2009). From the above, we can infer that the size of the fractured network of polygons is directly indicative of the thickness of the stressed zone.

The manner by which fractures intersect is also indicative of certain properties in the material as well as stress orientation and development. For instance, if the tensile stress is initially isotropic, the first cracks that develop follow sinuous and rather random paths, but they tend to intersect at right angles (orthogonal intersection or T-junctions). The resulting polygons are variable in size and shape. Further cracking produces smaller and more regular polygons. Patterns of the first type are usually termed "irregular random orthogonal polygons"; the second "regular random orthogonal polygons" (Lachenbruch, 1962). However, if the tensile stress is uni-directional, the first cracks tend to develop at right angles to the stress, forming a parallel system, and then subsidiary connecting cracks develop, outlining a rectilinear system of polygons. Such patterns are referred to as "oriented orthogonal polygons" (Lachenbruch, 1962).

Non-orthogonal fracture intersections are also common and are generally thought to develop in very homogeneous materials if stress is applied so rapidly (e.g., quick intense evaporation or diurnal thermal fluctuations) that cracks develop more or less simultaneously across the surface of the material. In this case, the intersections form "Y" junctions with angles close to 120° instead of 90°. Non-orthogonal polygons tend to be pentagonal or hexagonal and rarely exceed 1 m in width (Lachenbruch, 1962; Williams and Robinson, 1989 and references therein) since larger volumes are more likely to contain spatially-heterogeneous mechanical properties and defects. It should be noted that fracture patterns, including those caused by desiccation, may evolve from orthogonal to non-orthogonal or Y-junctions with repeated cycles of crack closure and re-opening (e.g., Jagla, 2004; Goehring et al., 2010; Goehring, 2013). These cycles would occur seasonally for example with thermal contraction polygons or by repeated wetting–drying cycles in the case of desiccation cracks. Therefore, the mode of crack intersection may also be used in certain cases as an indicator of the pattern's maturity.

To summarize the relevant points to this study, polygons formed by desiccation can be in the order of centimeters if the stressed region is a thin surficial layer as, for example, in the case of common mud cracks, or it can be in the order of hundreds of meters if the stressed region is thick enough to induce and support 10s of meters-deep cracks (e.g., El-Maarry et al., 2012). Generally speaking, small polygons (centimeters up to several meters in width) develop with high desiccation rates and thin stressed regions, which are conditions regularly associated with surface evaporation. In this case, factors such as temperature, solar irradiance, and wind activity, play a major role. As polygons get bigger and reach 10–100s of meters in size, the role of surface evaporation decreases and gives way to other factors such as the soil or sediment mineralogy, permeability and hydrological conditions such as groundwater activity.

2.3. Desiccation polygons on Earth

Desiccation polygons are ubiquitous on Earth and attain a wide range of sizes that varies by several orders of magnitude. The principles of the desiccation mechanism and fracture development, presented in Sections 2.1 and 2.2 respectively, give an insight into the reasons for this wide variability. While small polygons are rather ubiquitous on Earth and can form in many climates, the
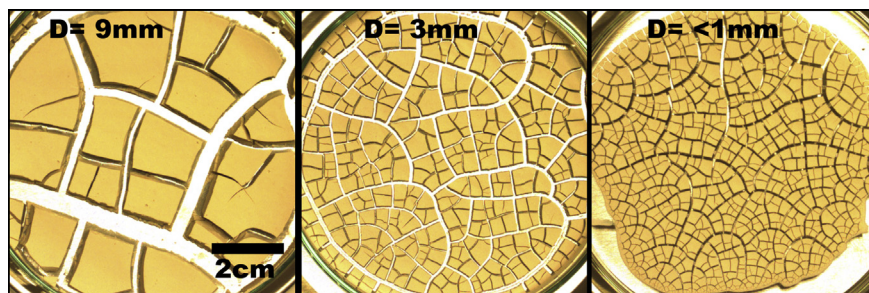

Fig. 1. Variation in size-scale of polygonal patterns with thickness (*D*) of desiccating material. Polygon size (i.e., crack separation) is directly dependent on the thickness of the stressed region (see text). The three figures show patterns in lab desiccation experiments (El-Maarry et al., in preparation) using the source clay Texas Montmorillonite STx-1, which is a Ca-rich montmorillonite (Costanzo and Guggenheim, 2001, and companion papers). All images are of the same scale. Samples have been left to desiccate freely in lab conditions at a stable temperature (~22 °C) and humidity range (30–35%) inside common glass Petri dishes.

larger polygons need special conditions to develop and are relatively rare occurrences (e.g., Neal et al., 1968; El-Maarry et al., 2012). However, since most PDPs on Mars have been detected by remote sensing instruments (i.e., are several to tens of meters-wide in general), a brief discussion of these larger desiccation polygons is presented.

It is important at this stage to note that there is a discrepancy in terminology between planetary science and terrestrial geology in regards to classifying polygonal crack patterns according to their size in general. On Earth, there are very few well-documented examples of what are termed "giant desiccation polygons" from the geological record (Loope and Haverland, 1988). Such polygons can be anywhere from 10s of meters-wide up to 300 m in size (Neal et al., 1968; Fig. 2). However, this size-range falls within the range termed intermediate-sized polygons on Mars (e.g., Seibert and Kargel, 2001; Mangold, 2005; El-Maarry et al., 2012) to differentiate it from the km-sized polygons of Utopia Planitia that are termed "giant" polygons (e.g., Pechmann, 1980). As such, these subjective terms should be used with caution.

Detailed field analysis by Neal et al. (1968) at 39 dried lakes and playas in the United States containing up to 300 m-wide desiccation polygons (Fig. 2) has shown that the sediments in these locations can often be more than 50 m thick and are composed of predominantly silt- and clay-rich lacustrine sediments containing clay minerals such as montmorillonite, illite, and vermiculite in addition to carbonates and analcites (Neal et al., 1968; Harris, 2004). These large features are proposed to form through the slow lowering of a water table rather than surface evaporation, which would permit the build-up of stress in thick beds within long time periods of 1–2 years (Neal et al., 1968). Most of these sites show a hierarchical arrangement of patterns from 10 to 100 of meters wide orthogonal polygons down to sub-meter-wide polygons displaying both orthogonal and Y-junctions.

2.4. Desiccation modeling: principles and challenges

An extensive body of work is present in the literature for modeling and experimental characterization of desiccation on Earth for civil engineering and agricultural purposes (e.g., Konrad and Ayad, 1997; Kodikara et al., 2004; Hu et al., 2006; Nahalawi and Kodikara, 2006; Peron et al., 2009a, 2009b; Amarasiri et al., 2010; Tang et al., 2011) since shrinking/swelling behavior and desiccation of clay-rich soils can create hazardous situations for civil structures and underground pipes. As such, many of the principles discussed here are developed from these models and have been presented in more detail by El-Maarry et al. (2012). The main aim of this section is to briefly lay down the foundations of desiccation modeling, which can hopefully be expanded upon in future studies.

Generally, the stress–strain relation for a desiccating saturated soil or sediment (i.e. all its voids are filled with water) takes the following differential form:

$$\dot{\varepsilon} = \frac{1+v}{E}\dot{\sigma} - \frac{1+v}{E^2}\frac{\partial E}{\partial w}\dot{w}\sigma + \alpha\dot{w} \tag{1}$$

where ε is the strain, v is Poisson's ratio, E is Young's modulus, σ is the stress, w is the gravimetric water content (wt%), and α is the hydraulic expansion coefficient (for complete derivation of the equations and model refer to El-Maarry et al., 2012). In this equation, the first two terms on the right hand-side represent the elastic components of the stress while the third term represents the hydraulic component. If the strain rate is set to zero, the equation is simplified into what is known as pre-fracture conditions. This simplification permits the computation of the stress buildup and possible onset of cracking but cannot model the crack propagation or evolution with time, which generally needs more complex methods such as finite element models. The morphological similarity of desiccation polygons and TCPs can be explained by the similarities
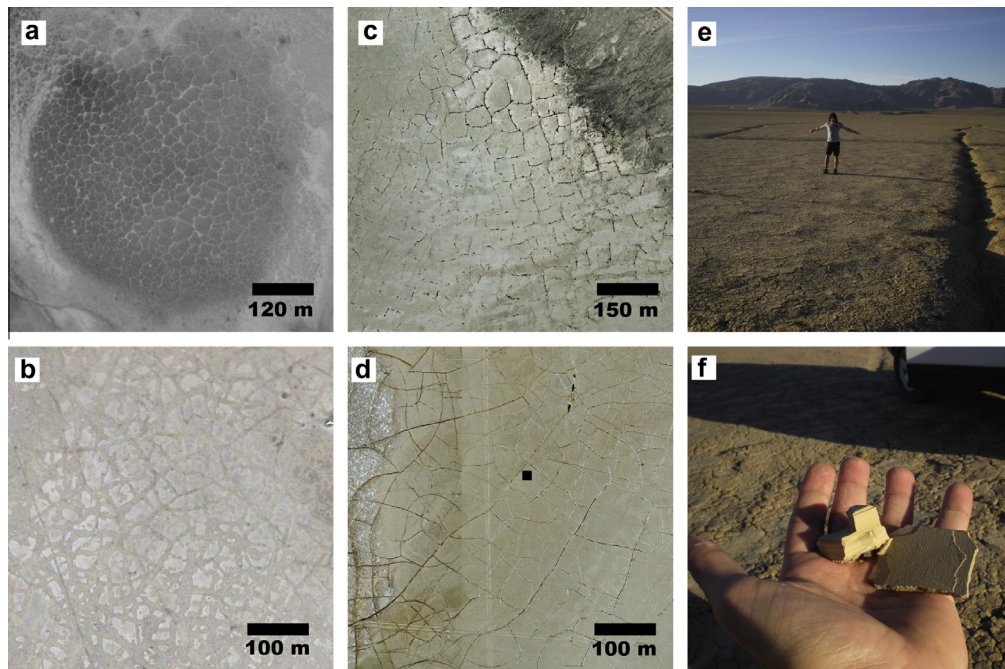

Fig. 2. Dried plains/playas on Earth (all located in California, US) that display tens of meters-wide desiccation polygons. (a) Deep Springs Valley playa (37.25°N, 118.03°W), which is a salt-rich playa (Neal et al., 1968; Lawrence et al., 1978) that usually hosts an ephemeral lake during the wet season (1998 image). This location is a potential analog to chloride-bearing terrains on Mars (see text). (b) Lavik playa (34.6°N, 116.3°W). (c) Coyote playa (35.1°N, 116.7°W). (d) Lucerne playa (34.5°N, 116.9°W). Black dot shows the approximate location of (e and f). (e) Large desiccation cracks in Lucerne playa (image taken in 2012). (f) A hand-sample of the playa surface material. Note the platy and sheet-like morphology, indicative of clay minerals, which are the main contributor to the development of large desiccation cracks on playa surfaces. Image credit for (a–d): Google Earth and the US Geological Survey. Figure adapted from El-Maarry et al. (2013a).

in their mathematical expression. For instance, a similar stress–strain relation for a frozen soil or unconsolidated sediment undergoing thermal contraction attains the simplified differential form (e.g., Mellon, 1997):

$$\dot{\varepsilon} = \frac{1+v}{E}\dot{\sigma} - \frac{1+v}{E^2}\frac{\partial E}{\partial T}\dot{T}\sigma + \alpha_T\dot{T} + \varepsilon_v \qquad (2)$$

where T is for temperature in Kelvin, α_T is the thermal expansion coefficient, and ε_v is the a viscous creep strain component. The first key difference between Eqs. (1) and (2) is the replacement of the hydraulic component with a thermal one along with the respective replacement of the shrinkage/expansion coefficient with the thermal expansion coefficient. In this case, temperature differences and thermal diffusivity of the soil replace the change in water content and soil diffusivity as the principle agents in stress generation/evolution (which are usually modeled in isothermal conditions). A second difference is the absence of a viscous creep component (ε_v) in the desiccation model. The reason for that is that whereas stress relaxation through creep is believed to be significant for ice-rich soils when temperatures are close to the melting point of ice, this is not the case with desiccation models where the temperatures are very often far below the melting points of any of the soil constituents (El-Maarry et al., 2012).

An important distinction between desiccation and thermal contraction processes lies in the difference between the hydraulic and thermal diffusivity components. Whereas thermal diffusivities of frozen soils are not expected to vary by orders of magnitude, this is not the case for hydraulic diffusivity, which can vary by orders of magnitude from clay-rich nearly impermeable soils to well-sorted sand-sized gravels. As a result, TCPs tend to have a limited size-range, whereas desiccation polygons can attain various shapes and sizes ranging from cm-sized up to 100s of meter-sized because of the larger variability observed within the soil properties and rate of desiccation.

Fig. 3 shows the results of running a desiccation model using Eq. (1) to assess the formation conditions of 100s of meter-sized desiccation polygons on Earth (El-Maarry et al., 2012). In this model, the rate of desiccation is assumed to be mainly controlled by the soil diffusivity and desiccation is assumed to evolve through lowering of the water table rather than surface evaporation. In this

case, the water loss can be described by Fick's second diffusion law (see El-Maarry et al., 2012):

$$\frac{dw}{dt} = D\frac{d^2w}{dz^2} \qquad (3)$$

where D is the diffusivity coefficient in m^2/s, and diffusion is assumed to be in the vertical direction z to simulate a lowering of the water table. Cracking is assumed to occur at the stage where the tensile stresses exceed the tensile strength of the desiccating soil (for the calculation method of the tensile strength and modeling of water table retreat, please refer to El-Maarry et al., 2012). The plotted results are for a range of diffusivities considered for both Earth and Mars. As expected, the tensile stress in all cases is shown to rise monotonically with time. The stress at a given time varies logarithmically following the variation in diffusivities. By examining Fig. 3, we can deduce that intermediate values between $10^{-2}\ m^2/s$ and $10^{-4}\ m^2/s$ create optimum conditions for the formation of cracks at the time scales suggested for the formation of giant desiccation polygons on Earth (Neal et al., 1968; 1–2 years). This diffusivity range agrees excellently with expected values of clay-rich sediments in general, which are usually in the range of 10^{-3}–$10^{-4}\ m^2/s$ (Domenico and Schwartz, 1998). Note that values above $10^{-2}\ m^2/s$ would lead to early ($\sim$20 days on Earth), and consequently shallow, fractures (i.e., small polygons). Extrapolating to the martian case yields similar results, but at longer time scales. For instance, cracking occurs after $\sim$500 days at diffusivities of $10^{-3}\ m^2/s$, as opposed to $\sim$200 days on Earth. This is expected since the only variable factor in this model is the gravitational constant ($\sim$3.7 m/s^2 on Mars vs. 9.8 m/s^2 on Earth), which results in slower rates of water table retreat (i.e., lower desiccation rates) on Mars for any given diffusivity compared to Earth.

To summarize, the generation of thick stressed regions is unlikely through fast desiccation rates (e.g., through surface evaporation) or high diffusivities, which would lead to shallower cracks and smaller desiccation polygons. Alternatively, slow desiccation rates can occur through simple gravitationally-induced lowering of the water table when the soils have low enough diffusivity values to control it as is the case with clay-rich soils or sediments (El-Maarry et al., 2012).

3. Global distribution of PDPs on Mars

Differentiating between polygon formation mechanisms using remote sensing and limited in-situ data has been, and remains, a difficult task because of the sole reliance on remote morphological investigations. For example, Mutch et al. (1976) favored thermal contraction as a mechanism for forming the polygons at the Viking 2 lander site. However, they could not rule out desiccation processes. This is not the case with km-sized polygons located in the Utopia basin. Several authors (e.g., Pechmann, 1980; McGill and Hills, 1992) have shown that thermal contraction and desiccation could not be responsible for the formation of km-sized polygons since that would involve a deep stressed zone (almost 500 m deep), which cannot be caused by thermal or desiccation tensile stresses. As such, they concluded that regional tectonic processes were most likely responsible for the formation of the polygons. Recently, Moscardelli et al. (2012) have suggested that such km-sized polygons could form in a marine-like subaqueous setting similar to deep water polygonal fault systems. In the case of smaller (10–200 m-sized) polygons, Baker (2001), for example, favored ice-wedging as a process for forming the 40–100 m-sized polygons that were observed in images from the Mars Orbiter Camera (MOC). Seibert and Kargel (2001) favored the same mechanism, but did not rule out desiccation.
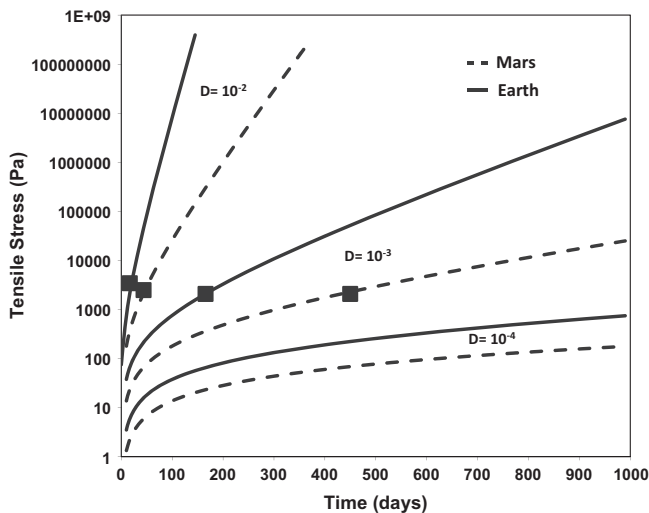
Fig. 3. Stress evolution in a desiccating soil with different diffusivities assuming desiccation by lowering of water table in a pre-fracture state under Earth- and Mars-like gravitational settings. Note the consistently longer durations computed for a martian setting compared to Earth. Black squares signify the corresponding onset of cracking for each case (if applicable). Figure adapted from El-Maarry et al. (2012).

Whereas a single dedicated global mapping investigation for PDPs is yet to be carried out on Mars, a picture is already emerging from the combination of numerous studies that have noted the presence of desiccation-like features, especially in association with phyllosilicate-bearing terrains. Fig. 4 shows a global inventory of locations that display PDPs. The dataset includes the subset of smectite-/vermiculite-bearing units as compiled by Carter et al. (2013) that display PDPs in addition to the numerous localities that have been mentioned in studies cited in this paper (e.g., El-Maarry et al., 2010, 2013a, 2013b). The geological units that contain PDPs are interpreted in Carter et al. (2013) and references therein to be of sedimentary origin and appear as horizontal beds, crustal units, or deltas/alluvial fans. In addition to these regions, PDPs are also present in association with chloride-bearing terrains, which on occasions are stratigraphically or regionally-associated with Fe/Mg phyllosilicate-bearing units (El-Maarry et al., 2013a, Section 3.2). Finally, the dataset also includes crack patterns that are present in many impact crater-floors (El-Maarry et al., 2010), which were suggested to form through desiccation (Section 3.3).

Overall, the global dataset of PDPs can be grouped into clusters that correspond to certain regions on Mars, which include Mawrth Vallis, Circum Isidis (Nili Fossae and Libya Montes), Margaritifer and Sirenum Terra, Eastern Valles Marineris, and northern cir-cum-Hellas. Below, we present a brief overview of the geological setting of the PDPs within these notable regions on Mars. A summary of this overview is listed in Table 1.

3.1. Phyllosilicate-bearing terrains

3.1.1. Mawrth Vallis

The largest areal exposures of phyllosilicate-bearing rocks on Mars occur on the plains surrounding Mawrth Vallis (Noe Dobrea et al., 2010). The region ($\sim 10^6$ km^2) has a consistent stratigraphy (Noe Dobrea et al., 2010) of Fe/Mg-smectite-bearing rocks overlain by Al phyllosilicate-bearing rocks, which is exposed both through erosion and on crater walls (Bibring et al., 2005; Poulet et al., 2005; Loizeau et al., 2007; Bishop et al., 2008; Wray et al., 2008; McKeown et al., 2009; Loizeau et al., 2010; Noe Dobrea et al., 2010, 2011). The Fe/Mg-smectite-bearing unit consists of two layers: a darker, underlying unit with weak spectral signatures (Loizeau et al., 2010) and a lighter layer with stronger signatures.

Spectra of the Al phyllosilicate layer are consistent with the presence of montmorillonite and isolated outcrops of kaolinite, both mixed with hydrated silica (McKeown et al., 2009, 2011), as well as instances of jarosite (Noe Dobrea et al., 2011). Both the Fe/Mg-smectite-bearing unit and the Al phyllosilicate-bearing unit exhibit fracturing that is consistent with desiccation (McKeown et al., 2013).

The Fe/Mg-smectite-bearing unit is fractured into irregular polygons 2–5 m across (Fig. 5) which are evident on all exposed surfaces, including crater walls (Bishop et al., 2008; Wray et al., 2008; Noe Dobrea et al., 2010; Loizeau et al., 2012; McKeown et al., 2013). McKeown et al. (2013) interpret the widespread distribution and geometry of the polygonal fractures to be most consistent with desiccation as the primary formation mechanism. In some locations, the crack patterns are superimposed or modified by other processes, such as impact craters, where parallel or radial fracture patterns are observed (McKeown et al., 2013).

The Al phyllosilicate-bearing unit (Fig. 5) is predominantly fractured into regular polygons 0.5–1.5 m across (Bishop et al., 2008; Wray et al., 2008; Noe Dobrea et al., 2010; Loizeau et al., 2012; McKeown et al., 2013) whereas some kaolinite-dominated regions are fractured irregularly, making larger polygons (McKeown et al., 2013) and regions displaying mineralogies consistent with hydrated silica exhibit less fracturing (Bishop et al., 2008). The fracturing in the Al phyllosilicate-bearing unit could also be dominated by desiccation processes; however, polygons are smaller and much more regular than the polygons that pervade the Fe/Mg-smectite-bearing unit (McKeown et al., 2013).

There is additional evidence for desiccation processes occurring in the Mawrth Vallis region. For example, large-scale sinuous cracks (100s of meters long) are observed on the floor of Mawrth Vallis (Fig. 6) that are remarkably analogous to giant desiccation features in dry playas on Earth (Section 2.3, Fig. 7). Finally, patterns resembling PDPs are also visible in sulfate- and sulfate/phyllosilicate-bearing terrains. For instance, Farrand et al. (2009) identified jarosite, a sulfate, on the plains above Mawrth Vallis and noted the similarity between the fractures observed in the jarosite-bearing rocks and those in Fe/Mg-smectite-bearing rocks. They proposed that the evaporation of an ephemeral lake or a groundwater pond could account for this deposit. Also, Wray et al. (2010) identified Ca-sulfate bassanite in polygonally-fractured deposits in the floor of Mawrth Vallis in association with, and underlying, Fe/Mg
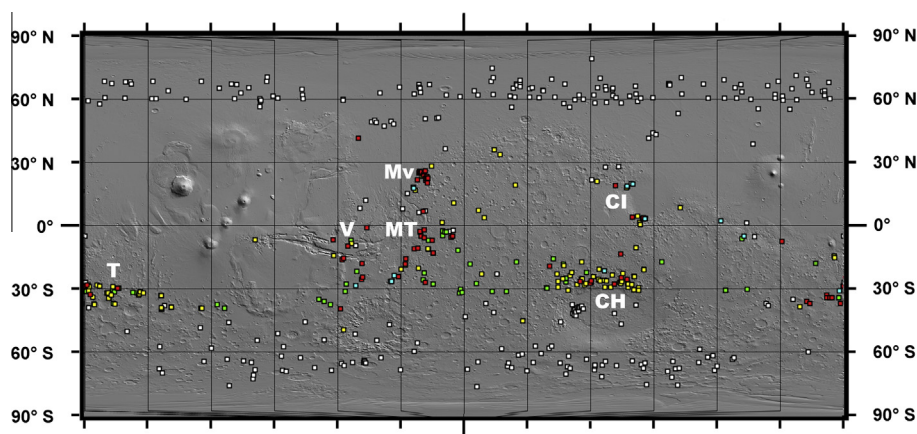

Fig. 4. MOLA-based shaded relief map for the surface of Mars containing locations of PDPs. The dataset includes crack patterns in smectite-bearing deposits that are observed either in horizontal beds (yellow), crustal outcrops (red), or deltas/alluvial fans (light blue), which are a subset of Carter et al.'s (2013) dataset of hydrous-rich terrains on Mars. Also included are the crack patterns in chloride-bearing terrains (El-Maarry et al., 2013a, green) as well as patterns in impact crater floors as reported by El-Maarry et al. (2010, white). PDPs are clustered in certain localities in the southern highlands, which include Mawrth Vallis (Mv), Terra Sirenum (T) and Margaritifer Terra (MT), Eastern Valles Marineris (V), circum-Isidis (Nili Fossae and Libya Montes, CI), and northern circum-Hellas (CH). (For interpretation of the references to color in this figure legend, the reader is referred to the web version of this article.)

Table 1

Summary of notable provinces of Mars that display PDPs. See Section 3 for more detail.

Mars locality	Mineralogy	PDP setting	References on mineralogy
Mawrth Vallis	Fe/Mg smectite-bearing rocks overlain by Al-phyllosilicate-bearing layer Additional exposures of sulfate/ phyllosilicate bearing rock and bassanite	Small 0.5–5 m-wide polygons but also includes some of the largest PDPs on Mars. Polygons in Fe/Mg smectites generally larger than ones in Al-phyllosilicates	Bibring et al. (2005), Poulet et al. (2005), Loizeau et al. (2007), Bishop et al. (2008), Wray et al. (2008, 2010), McKeown et al. (2009, 2013), Farrand et al. (2009), Loizeau et al. (2010), Noe Dobrea et al. (2010, 2011)
Nili Fossae	Nontronite-rich phyllosilicates, which probably predate Isidis impact Exposures of Serpentine, chlorite, prehnite, illite, kaolinite as well as olivine, pyroxene and carbonates	Usually degraded and obscure. Limited in spatial distribution. Mainly in association with smectites but fractures are also visible in olivine- and carbonate-bearing deposits	Poulet et al. (2005), Mangold et al. (2007), Mustard et al. (2007, 2009), Ehlmann et al. (2008a, 2008b, 2009, 2010)
Libya Montes	Fe/Mg-rich smectites, Al-smectite, olivine–smectite–carbonates assemblages	Fe/Mg bearing outcrops Al-smectites in deltas Olivine–smectite–carbonate assemblages	Mustard et al. (2007), Tornabene et al. (2008), Erkeling et al. (2012), Bishop et al. (2013a)
N. circum Hellas	Sedimentary deposits containing Fe–Mg smectite/chlorite mixed layers and uplifted crustal material that contains hydrothermal assemblages of prehnite/ chlorite	Several meters wide in association with thick sedimentary deposits containing Fe/Mg smectite–chlorite mixed layers	Noe Dobrea and Swayze (2012)
Terra Sirenum	Fe/Mg smectites in plains	In association with Fe/Mg smectites in all settings as well as the chloride-bearing terrains	Murchie et al. (2009), Wray et al. (2009, 2011); Wendt et al. (2013); Glotch et al. (2010)
	Chloride-bearing terrains Phyllosilicates knobs and layers interbedded with sulfates in impact craters	Features are usually fresh looking and appear to be recently exhumed	
Margaritifer & Eastern Valles Marineris	Numerous discontinuous exposures of Fe/Mg phyllosilicates overlain by Al-phyllosilicates	In association with Fe/Mg smectites. Most features appear degraded or pervasively fractured	Di Achille et al. (2009), Wintzer et al. (2011), Le Deit et al. (2012)
Chloride-bearing terrains	Chloride-bearing materials sometimes in association with Fe/Mg phyllosilicates	In association with Fe/Mg smectites but also in other chloride-bearing g deposits that lack a phyllosilicate signature	Osterloo et al. (2008, 2010), Glotch et al. (2010), Ruesch et al. (2012), El-Maarry et al. (2013a)
Crater-floor polygons[a]	N/A	Features concentrated in craters in the high latitudes. They have a variable size of 70–350 in width. Possibly needs a complex interplay between desiccation and thermal contraction	N/A
In-situ observations by rovers	Meridiani: Light-toned aeolian sandstones containing sulfates	Meridiani: cm- to m-sized polygons that display both Y and T junctions in association with deposits interpreted to eolian sandstones	McLennan et al. (2005)
	Gale crater: light-toned mudstones that contain ∼20 wt% of smectites in addition to sulfates, sulfides and amorphous contents	Gale: Polygonal patterns that range in size from <1 m- to 20 m-wide patterns	Vaniman et al. (2014)

[a] As described by El-Maarry et al. (2010).

phyllosilicates-bearing materials, which they interpret to indicate a complex hydrological history.

3.1.2. Circum-Isidis: Nili Fossae and Libya Montes

The Noachian-aged southern highlands terrain bordering the southern margin of Isidis Planitia basin rim, Libya Montes, is one of the most fluvially-modified ancient terrains on Mars and contains one of the highest densities of valley networks on Mars (Crumpler and Tanaka, 2003). In contrast, the Nili Fossae region, which lies north of the Syrtis Major volcanic complex and west of Isidis, has been an area of volcanologic and tectonic interest (e.g., Schaber, 1982), especially ever since the thermal infra-red observation of olivine-bearing rocks (Hoefen et al., 2003). Both regions surrounding Isidis display various phyllosilicate signatures and interesting mineralogies, yet have different geologic settings. Therefore, they are discussed here together for comparison.

i. Nili Fossae

The Nili Fossae region contains large exposures of phyllosilicates, mainly nontronite-rich (e.g., Poulet et al., 2005; Mangold et al., 2007; Ehlmann et al., 2009), which probably predate the formation of the Isidis basin (Mustard et al., 2007, 2009). In addition to nontronite, several other phyllosilicates are observed, including serpentine, chlorite, prehnite, illite and kaolinite (Ehlmann et al., 2009, 2010), as well as carbonates (Ehlmann et al., 2008a,

2008b), olivine (Hoefen et al., 2003; Mustard et al., 2005), and pyroxene (Mustard et al., 2005). An interesting attribute of many of these phyllosilicates is their inferred formation under elevated temperatures (Ehlmann et al., 2009, 2010).

Despite the large exposures of Noachian crust and phyllosilicates in Nili Fossae, crack patterns (Fig. 8) are relatively uncommon. There are a number of reasons that can account for this trait: (1) the phyllosilicates comprise the lowest compositional unit that was laid down before the Isidis impact. As a result, this unit is now complex and heavily brecciated (Mustard et al., 2009), which may have contributed to erasing pre-existing crack patterns, (2) high temperature formation or thermal processing of the altered units containing illite, chlorite, serpentine, and/or chlorite (Ehlmann et al., 2009, 2010), and (3) diagenesis or hydrothermal alteration, which may indeed have contributed to the formation of carbonates and serpentines (e.g., Brown et al., 2010; Viviano et al., 2012).

It should be noted that crack patterns in Nili Fossae are observed not only in smectites, but also in carbonate-bearing deposits (Ehlmann et al., 2008a, 2008b; Fig. 8) and in weathered olivines and serpentines (Ehlmann et al., 2010). Carbonates are known to exhibit desiccation patterns similar to smectites but to a lesser degree (e.g., Baria, 1977). Nonetheless, it is possible that the lithified units containing a spectrally dominant signature of carbonates may contain considerable amounts of smectites as well. Indeed, all carbonate exposures in Nili Fossae are also associated
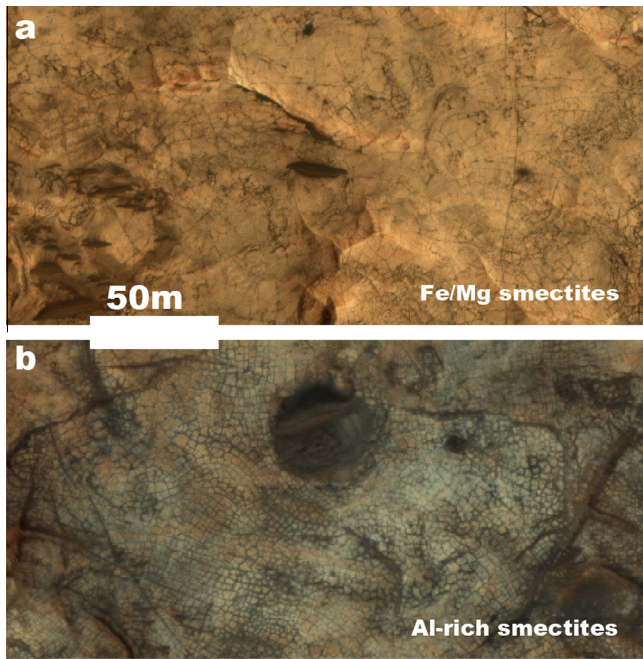
Fig. 5. Fracture patterns in Mawrth Vallis are generally observed in Fe/Mg smectites (a) and Al-rich smectites (b). The Mawrth region has a consistent stratigraphy of Fe/Mg-smectite-bearing rocks overlain by Al phyllosilicate-bearing rocks, which is exposed both through erosion and in crater walls. *Source:* HiRISE color products with Image IDs: (a) PSP_007612_2045, (b) PSP_005964_2045. Images credit: University of Arizona/JPL/NASA.
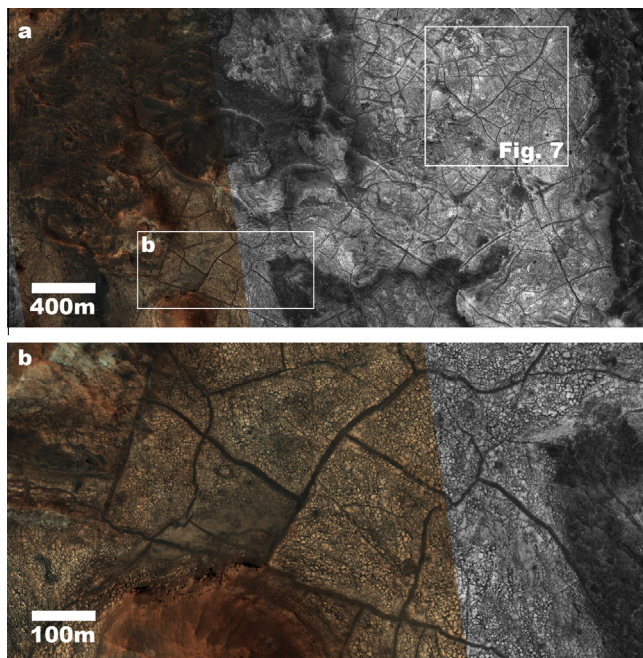

Fig. 6. Some of the largest PDPs on Mars in an Fe/Mg-bearing unit exposed on the floor of Mawrth Vallis. The PDPs display fractal-like fracturing with the largest fractures forming long sinuous patterns that are further intersected by smaller fractures. Applying the principles of tensional cracks that were discussed in Section 2 suggests that the Fe/Mg bearing units in this location have a minimum thickness of 10–30 m. *Source:* HiRISE merged RGB product with Image ID: PSP_006755_2030. Image credit: University of Arizona/JPL/NASA.

with Fe/Mg smectites, sometimes with indistinguishable stratigraphical boundaries (Ehlmann et al., 2008a, 2008b). In addition, a laboratory mixture of Mg-rich carbonate (80 wt%), olivine

(15 wt%), and nontronite (5 wt%) produces a spectrum similar to that observed by CRISM in Nili Fossae (Ehlmann et al., 2008a, 2008b). Similarly, CRISM data indicate that the olivine-rich bedrock compositions in locations of olivine–carbonate–serpentine assemblage are heterogeneous, exhibiting partial alteration in most places to magnesium carbonate and, in other places, to serpentine (Ehlmann et al., 2010). However, smectites could also be available as an alteration product possibly masked by stronger spectral signatures from the other components.

ii. *Libya Montes*

Libya Montes is situated in the southern margin of the Isidis Planitia rim. It is one of the oldest and most extremely eroded surfaces on Mars (Jaumann et al., 2010). This region is greatly modified by impact, volcanic, tectonic, aeolian, and fluvial processes (Scott and Tanaka, 1986; Crumpler and Tanaka, 2003; Erkeling et al., 2010; Jaumann et al., 2010). Libya Montes and the southern Isidis region host dense valley networks that incise into terrain dating from the Noachian, Hesperian and Amazonian periods (Crumpler and Tanaka, 2003; Mustard et al., 2007; Tornabene et al., 2008; Erkeling et al., 2010; Jaumann et al., 2010).

Libya Montes hosts Noachian to Amazonian aged surface rocks with extensive outcrops of olivine- and pyroxene-bearing material that appear to be morphologically, spectrally and stratigraphically related to Nili Fossae (Bishop et al., 2013a). It also features surface outcrops and/or deposits hosting Fe/Mg smectite, Fe/Mg-smectite mixed with carbonate and/or other Fe/Mg-rich phyllosilicates, and Al-smectite (Bishop et al., 2013a). These units likely formed through chemical alteration connected with hydrothermal activity resulting from the formation of the Isidis Basin and/or the pervasive fluvial activity throughout this region (Bishop et al., 2013a). As in Nili Fossae, all carbonate exposures at Libya Montes are also associated with Fe/Mg smectites and olivine (Bishop et al., 2013a).

Polygonal crack patterns are common in this region (Fig. 9) and are especially abundant, for example, in Al-rich smectites in distal parts of potential deltas (Erkeling et al., 2012, Fig. 9a), in Fe/Mg-rich phyllosilicate outcrops in impact craters such as Hashir crater and its surroundings, as well as olivine–smectite–carbonate assemblages (Bishop et al., 2013a; Fig. 9b and c). Some phyllosilicate-bearing units in Libya Montes show similarly brecciated units with putative or no crack patterns which, as in the case of Nili Fossae, may indicate either heavy modification by the Isidis impact event, a hydrothermal genesis, or both (see also Bishop et al., 2013a). Other units consistent with olivine lithology also exhibit polygonal cracks (Tornabene et al., 2008; Bishop et al., 2013a). However, for these patterns to be considered PDPs, we would have to assume that a small degree of alteration not visible from orbit is present along with olivine in these outcrops.

3.1.3. Terra Sirenum

The Terra Sirenum region contains some of the oldest stratigraphical units on Mars with multiple exposures of phyllosilicates- and chloride-bearing deposits (Fig. 10). It hosts a variety of geological landforms that include Ma'adim Vallis, and multiple degraded basins that have been proposed to host paleolakes (e.g., Irwin et al., 2004; Howard and Moore; 2004; Davila et al., 2010; Wray et al., 2011). These lakes may have been isolated lakes or part of a larger lake, informally called Eridania, which could have formed Ma'adim Vallis (Irwin et al., 2004). In addition, the region contains multiple exposures of the Electris deposits, which are interpreted to be volcanic loess material (Grant and Schultz, 1990; Grant et al., 2010) and evidence for volcanic- (in the form of ridged plains) and tectonic- (in the form of extensive fault systems) activity, which may record the development of the Tharsis magmatic complex (e.g., Anderson et al., 2001; Dohm et al., 2001).
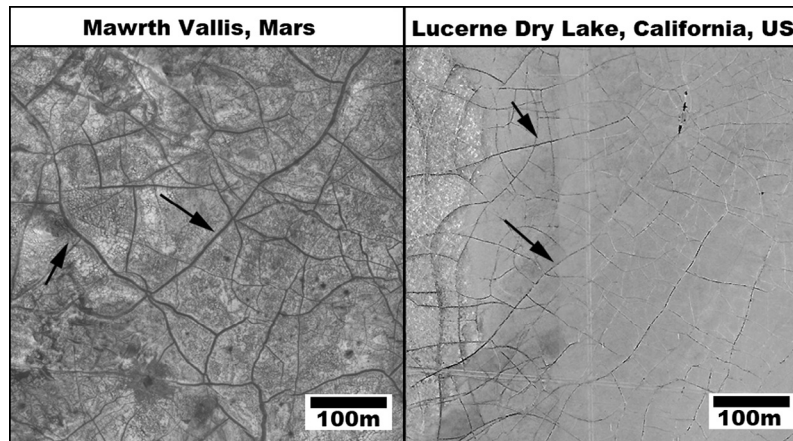
Fig. 7. Comparison between large features on the floor of Mawrth Vallis (left, HiRISE image PSP_006755_2030) and the large desiccation features in Lucerne Dry Lake in California, US (34.5°N, 116.9°W, see also Fig. 2). Note the exceptional similarities between the patterns in terms of morphology, size and crack propagation. Arrows point to the longest and largest sinuous fractures in both locations, which are thought to have formed first and later subdivided and intersected by the smaller fractures. Image credits: University of Arizona/JPL/NASA (left) and Google Earth (right).
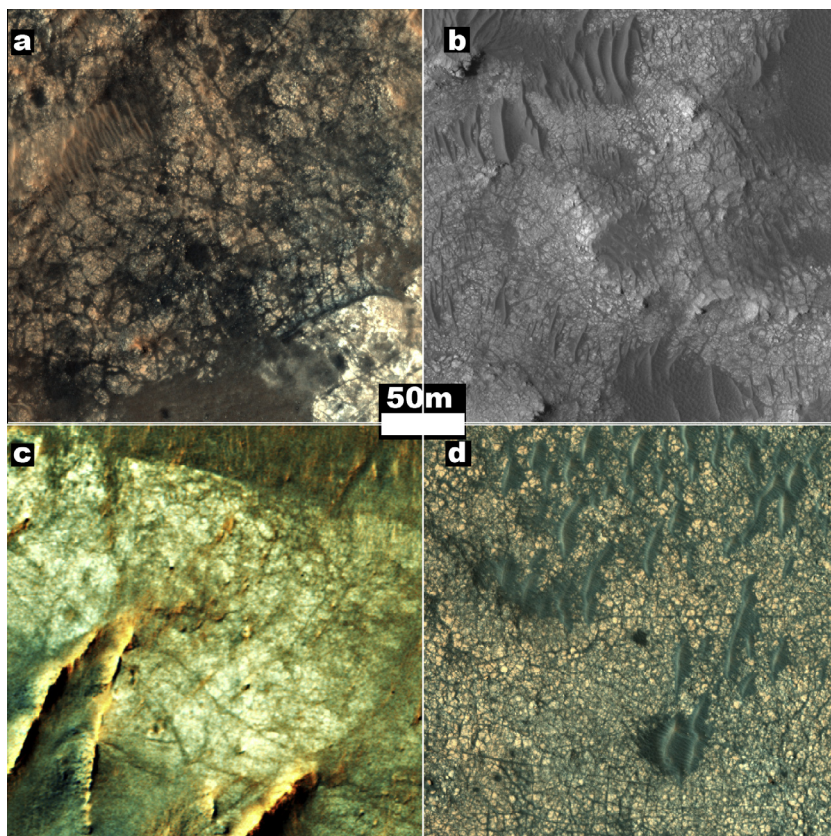

Fig. 8. Polygonal crack patterns in Nili Fossae. Crack patterns are usually visible with various states of preservation in Fe/Mg-phyllosilicate-bearing units (a–c) and are also observed in carbonate-bearing units (d). *Source*: Color and Red-filter HiRISE images with image IDs: (a) ESP_016575_1980, (b) PSP_002387_1985, (c) ESP_026478_2015, and (d) PSP_002532_2020. Images credit: University of Arizona/JPL/NASA.

Phyllosilicates are widespread in Terra Sirenum and have various settings. Fe/Mg smectites are common in inter-crater plain sediments and are occasionally associated with chloride-bearing materials (Murchie et al., 2009; Wray et al., 2009; Glotch et al., 2010; Ruesch et al., 2012; El-Maarry et al., 2013a, Section 3.2), which in turn, are concentrated in Sirenum (Osterloo et al., 2010). Phyllosilicates are also observed interbedded with sulfate layers in impact craters such as Columbus crater (Wray et al., 2011). Common intra-crater assemblages include Fe/Mg smectites,

montmorillonites, kaolinites, jarosite, alunite and ferric oxides (e.g., Wray et al., 2011). Finally, phyllosilicates are also common in outcrops within the numerous knobby (also named chaotic) terrains (Grant and Schultz, 1990) and are mainly composed of Fe/Mg-bearing and Al-rich phyllosilicates (Wendt et al., 2013).

Polygonal crack patterns are observed in all the above-mentioned settings, especially in association with chloride-bearing materials (Osterloo et al., 2010; El-Maarry et al., 2013a, Section 3.2). The ubiquitous presence of crack patterns within
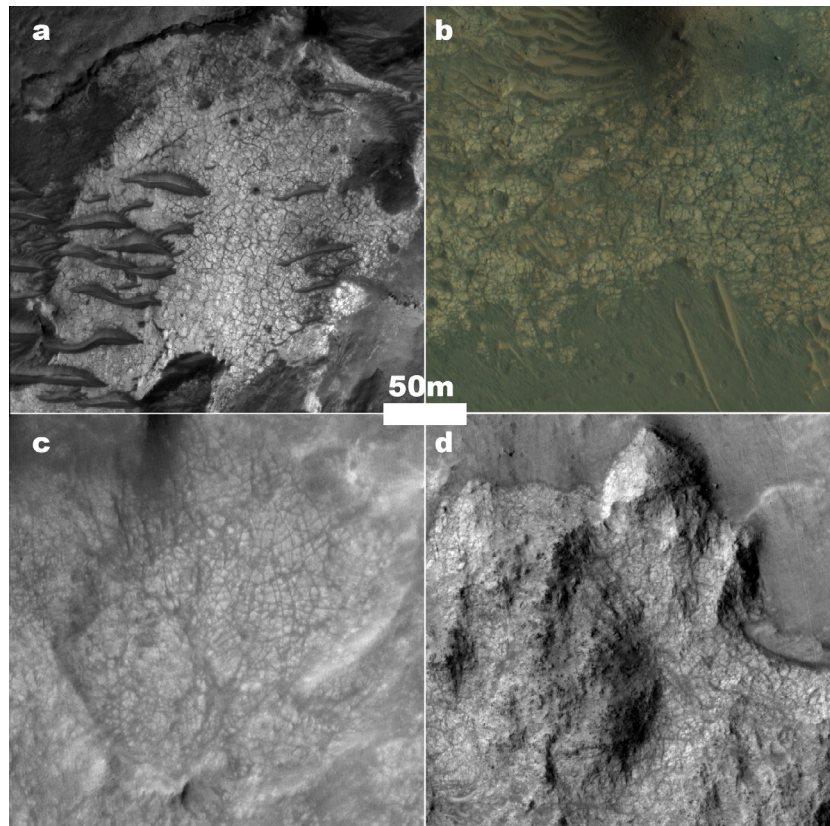
Fig. 9. Polygonal crack patterns in Libya Montes are observed in different settings that include (a) Al-rich smectites in fan deposits, (b) possible phyllosilicate-bearing deposits in the floor of Hashir crater, (c) Fe/Mg smectite/bearing deposits in outcrops east of Hashir crater, (d) olivine–carbonate–Fe/Mg smectite assemblage unit east of Hashir crater. Note the degraded and subdued features in comparison to other locations shown. *Source*: Color and Red-filter HiRISE images with image IDs: (a) PSP_008808_1830, (b) PSP_002756_1830, (c) ESP_017656_1835, and (d) ESP_016034_1835. Images credit: University of Arizona/JPL/NASA.
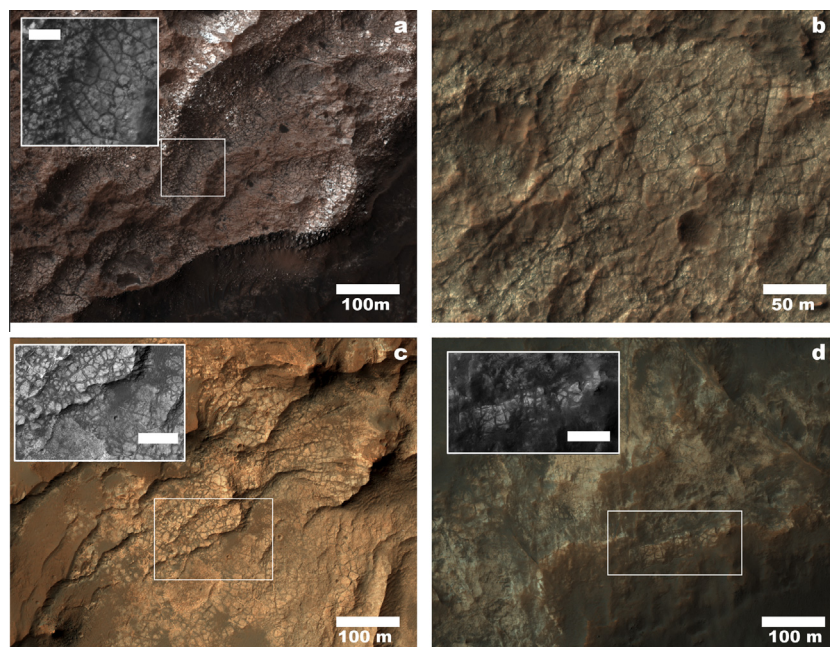

Fig. 10. Polygonal crack patterns in Terra Sirenum in HiRISE false RGB composites (insets are higher resolution sub-images with the red filter alone for clarity): (a) Intra-crater deposits in Columbus crater. The patterns are associated with Fe/Mg phyllosilicates, montmorillonites and sulfates (Wray et al., 2011). (b) Chloride-bearing terrains. (c) Light-toned deposits close to knobby terrain showing spectral signatures of Mg-rich phyllosilicates and weakly hydrated minerals (Wendt et al., 2013). (d) Less obvious, yet still visible, patterns in a mound in the knobby terrain. Similar knobs display signatures of Fe/Mg smectites and montmorillonites (Wendt et al., 2013). All scale bars in inset boxes are 50 m-wide. Image IDs: (a) ESP_013960_1510, (b) PSP_010387_1485, (c) PSP_006893_1515, and (d) PSP_005522_1450. Images credit: University of Arizona/JPL/NASA.
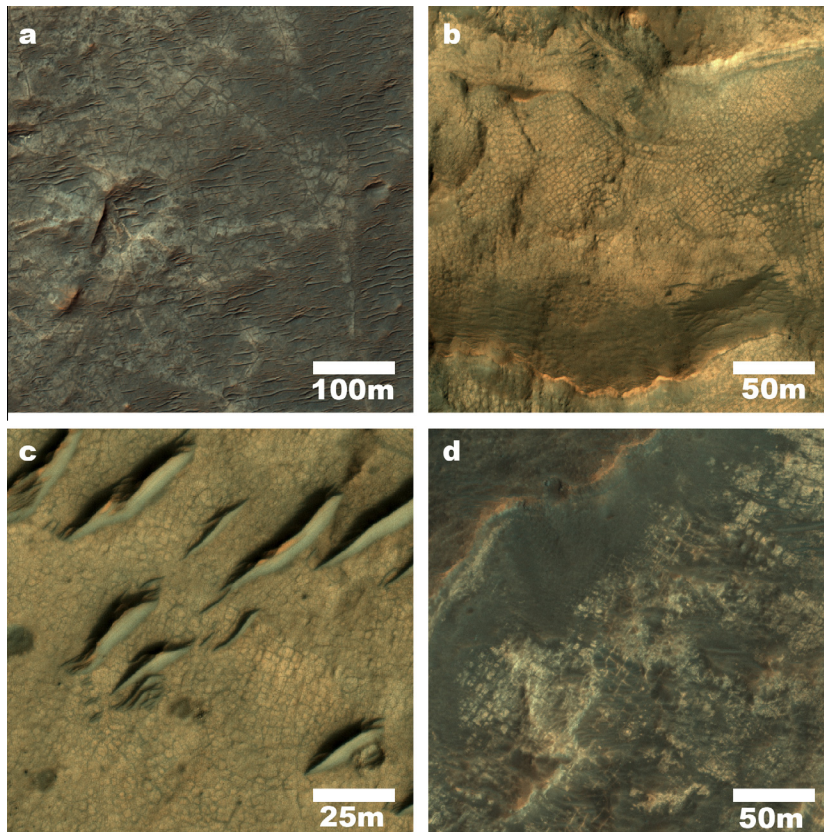
Fig. 11. Polygonal cracks in northern circum-Hellas region. Polygonal crack patterns are visible in Fe/Mg smectite/chlorite mixed-layer sedimentary deposits similar to other units on Mars. *Source*: HiRISE Color image products with image IDs: (a) ESP_024922_1570, (b) ESP_016259_1535, (c) ESP_16668_1555, and (d) ESP_013345_1540. Images credit: University of Arizona/JPL/NASA.

the Terra Sirenum deposits is consistent with the inferred rich aqueous history of these terrains that includes groundwater upwelling for the formation of intra-crater deposits (Wray et al., 2011) and many chlorides–phyllosilicates assemblages (Murchie et al., 2009; Wray et al., 2009; Glotch et al., 2010; Ruesch et al., 2012; El-Maarry et al., 2013a), and possibly sub-aqueous alteration beneath lakes for the formation of the phyllosilicates in the knobby fields (Wendt et al., 2013).

3.1.4. Northern circum-Hellas

The terrains associated with the circum-Hellas region exhibit a great diversity of geological environments including volcanic, glacial, hydrothermal, alluvial, and potentially lacustrine. Geological maps generated for the region identify terrains ranging in ages from Early Noachian through Hesperian. Investigations of the Northwestern circum-Hellas region reveal hydrated minerals in two specific rock units (Noe Dobrea and Swayze, 2012): sedimentary deposits associated with pitted plains and craters, and hydrothermally-altered material associated with ancient crustal rocks uplifted by the Hellas impact.

The sedimentary deposits consist of thick (200–500 m-thick) sequences of boulder- and yardang-forming layered units. These deposits occur both on the plains as well in the interior of craters, and are characterized by erosional pits that expose their layering. Stratigraphically, they embay older massifs and hills in the region. Near-Infrared CRISM spectra of these units are interpreted to be consistent with Fe/Mg smectite/chlorite mixed-layer materials. Texturally, these units exhibit fracture patterns similar to those observed in other Fe/Mg smectite units on Mars (Fig. 11). The polygons formed by these fractures are typically several meters in size and do not exhibit any preferred shape or orientation.

The hydrothermal units are associated with some of the hills found in the northwest Hellas region. These hills have been interpreted by Leonard and Tanaka (2001) to be uplifted crustal material and ejecta from the Hellas impact. Stratigraphically, they underlie all other units in the region. CRISM spectra of these units are consistent with the presence of prehnite/chlorite assemblages, and in some cases the spectra of these units are also consistent with muscovite or illite. The particular surfaces associated with these hydrothermal products tend to be expressed either as rough outcrops or smooth ripple-forming surfaces, implying that these materials are breaking down into sand-size particles that can be transported by wind via saltation. Texturally, the surfaces of the outcrops do not exhibit polygonal fracturing patterns, but instead appear rough with occasional fractures crosscutting the deposits.

3.1.5. Margaritifer Terra and Eastern Valles Marineris

The Margaritifer region contains various lines of evidence for past hydrological activity, which include numerous and well-preserved valley networks and channels such as Uzboi–Nirgal–Ladon, Samara, and Parana-Loire valley systems along with associated basins (Grant and Parker, 2002), and many impact craters that display evidence in their interiors for a rich hydrological history such as deltas, sedimentary layers and hydrous mineral-bearing outcrops. Notably, three of such craters (i.e., Miyamoto, Holden, and Eberswalde) were considered as candidate landing sites for the Mars Science Laboratory (MSL) Rover (Golombek et al., 2012). In Margaritifer Terra, numerous discontinuous exposures of Fe/Mg phyllosilicates are observed over the plateaus and occasionally within Margaritifer Chaos. The plateau phyllosilicates appear as discontinuous deposits outcropping from the plains unit. These are well identifiable in nighttime infrared data as they exhibit a
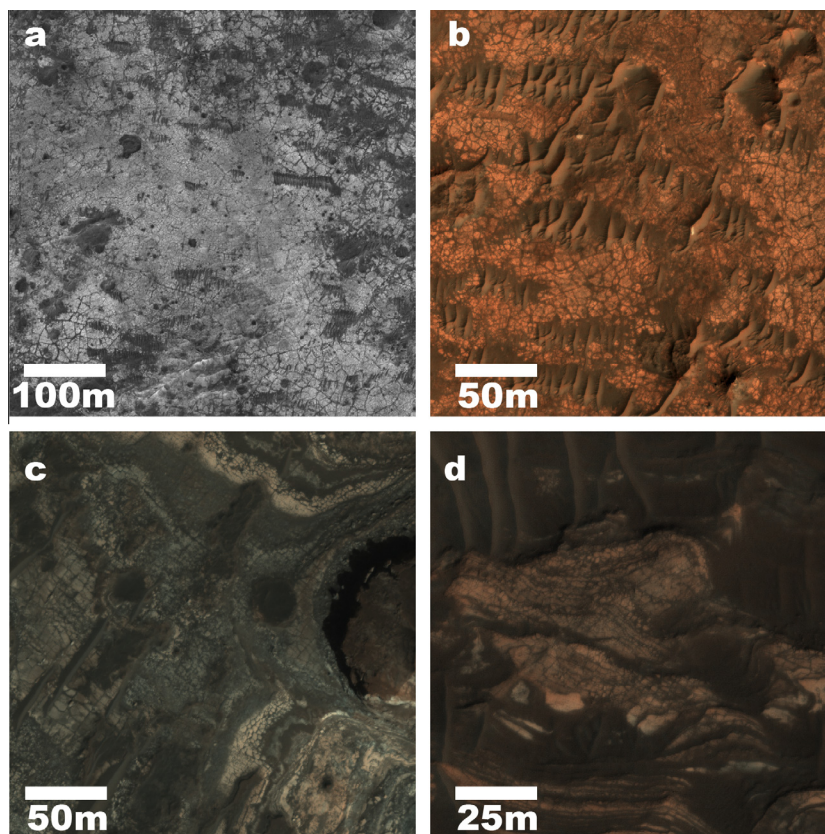
Fig. 12. Polygonal patterns in Fe/Mg-bearing phyllosilicates in (a and b): the Margaritifer region, (c) Eastern Vallis Marineris in Coprates Catena (see Grindrod et al., 2012), and (d) Shalbatana Vallis. *Source*: Color and Red-filter HiRISE images with image IDs: (a) ESP_013849_1750, (b) ESP_017739_1770, (c) PSP_007917_1650, and (d) PSP_008391_1790. Images credit: University of Arizona/JPL/NASA.

locally very high thermal inertia. The rugged and discontinuous texture of the outcropping deposits suggest intense erosion occurred after deposition, such that a much more extensive unit likely existed during the Noachian. At the HiRISE scale, the numerous identified outcrops exhibit polygonal fractures at the several meters scale (Fig. 12).

West of Margaritifer, Eastern Valles Marineris also displays numerous outcrops and sedimentary deposits that exhibit polygonal fractures resembling PDPs (Fig. 12). The outcrops are located along the plateaus surrounding Vallis Marineris and are mainly composed of Fe/Mg smectites and vermiculite as a lower member overlain by Al-rich smectite member with localized signatures of kaolinite and halloysite (Le Deit et al., 2012). A notable site in this region is Shalbatana Vallis, which displays geological and mineralogical evidence for ancient lake shorelines and paleolacustrine deposits (e.g., Di Achille et al., 2007, 2009; Wintzer et al., 2011) as well as PDPs, although the irregular patterns may be attributed to other mechanisms as well (e.g., tectonic, Fig. 12d). Indeed, most of the polygonal patterns in the Eastern Vallis Marineris region are either pervasively fractured or degraded, which may indicate long periods of exposure to weathering processes as opposed to being more recently exhumed.

3.2. Chloride-bearing terrains

The chloride-bearing terrains are a global distribution of predominantly polygonally fractured terrains that encompass many of the regions that have already been discussed (notably, Terra Sirenum). However, their unique mineralogical association with chloride-bearing deposits merits a brief overview. Osterloo et al. (2008, 2010) identified and mapped a spectrally-distinct compositional unit using data from the Mars Odyssey Thermal Imaging System (Christensen et al., 2004) and the Mars Global Surveyor Thermal Emission Spectrometer (Christensen et al., 2001). These materials are scattered within the southern highlands in >600 locations, yet are significantly concentrated in Terra Sirenum (Figs. 4 and 11, Section 3.1.3). They are composed of light-toned materials that are occasionally polygonally-fractured (Fig. 13), and lie within topographical depressions in typically low-albedo terrains of Noachian or Early Hesperian age. Their morphologies and thermal inertia indicate that they are relatively consolidated materials. The combination of these attributes led Osterloo et al. (2008) to conclude that these units were chloride-bearing materials that could have formed by precipitation from evaporating surfaces, such as saline lakes, groundwater/hydrothermal brines (as volcanic sublimates), or by direct efflorescence (Osterloo et al., 2008, 2010).

El-Maarry et al. (2013a) analyzed high resolution visible images and spectral data from the HiRISE and CRISM instruments, respectively, to characterize the surface textures associated with the chloride-bearing terrains in >80 locations. Their analysis reveals that 75% the regions display polygonal crack patterns associated with, or in proximity to, the chloride-bearing materials. Almost a third of the studied chloride-bearing terrains also display spectral signatures of Fe/Mg-rich smectites (El-Maarry et al., 2013a). The polygonal crack patterns generally resemble the patterns observed globally in this study. Within the framework of a desiccation hypothesis, El-Maarry et al. (2013a) conclude that the polygonal patterns are a direct indication of the presence of smectites in all locations that show crack patterns based on their resemblance to
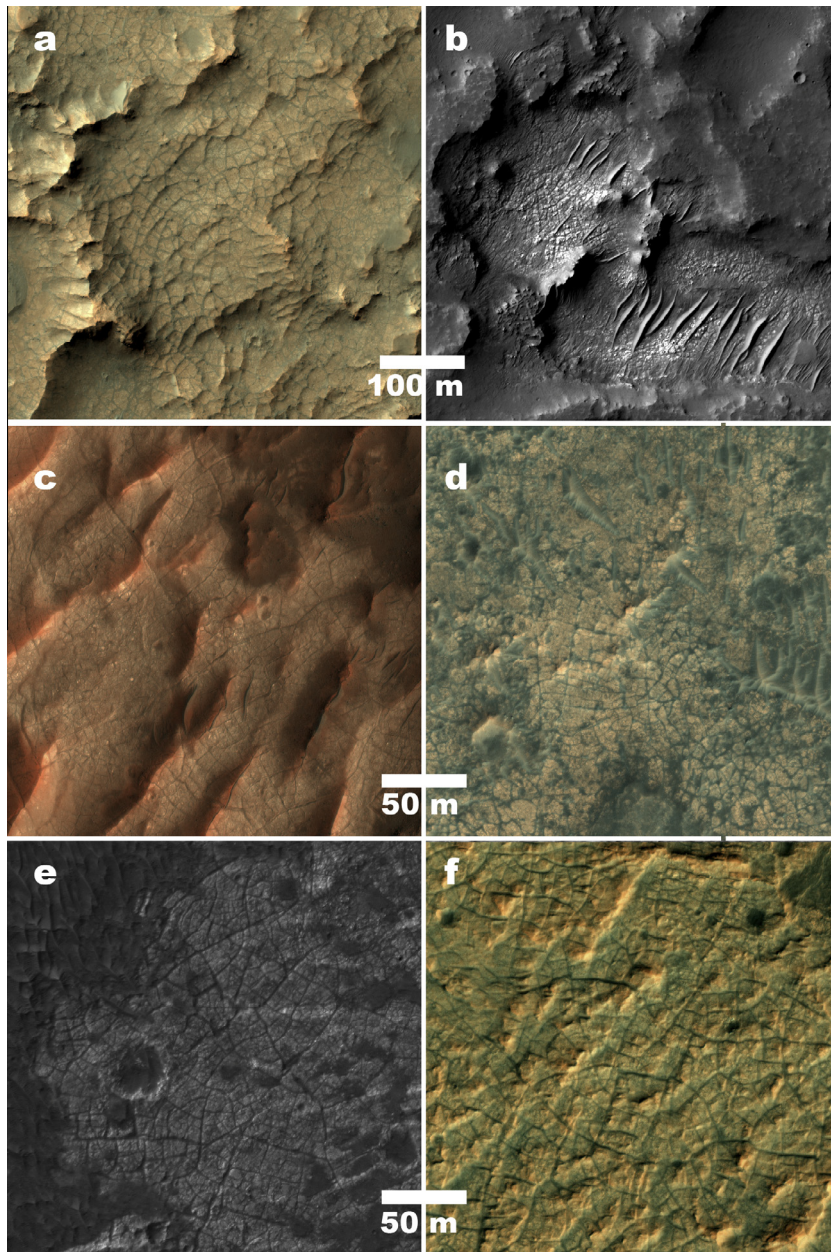
Fig. 13. Typical polygonal cracks associated with chloride-bearing deposits. The cracks are generally 1–2 m-wide and intersect in an orthogonal system to form polygons that typically measure 5–30 m in width. They tend to occur in relatively bright deposits that may appear on exhumed outcrops or ridges (a), within natural depressions (b), or as plain materials (c–f). The cracks show a continuum in terms of preservation or "freshness" that ranges from well-preserved (c) to degraded (d). Occasionally, the cracks are filled with dusty material (d) or covered by dunes/ripples (b), and in several cases the entire patterns may be obscured by dusty mantles (e). *Source*: Color and Red-filter HiRISE images with image IDs: (a) ESP_016057_1515, (b) ESP_018831_1545, (c) PSP_003160_1410, (d) ESP_016354_1745, (e) ESP_028197_1580, and (f) PSP_008917_1770. Images credit: University of Arizona/JPL/NASA.

polygonal patterns in dried lakes and playas on Earth in terms of size-scale and geologic setting. To address the lack of spectral evidence, they suggest that high salt concentrations, overlying dust covers, or thick indurated mantles/crusts (either chloride-bearing or spectrally featureless) may be responsible for obscuring the spectral signatures of the smectite clays in the fractured chloride-bearing terrains. Several studies (Osterloo et al., 2008, 2010; Glotch et al., 2010; Ruesch et al., 2012; El-Maarry et al., 2013a) suggest that salt-rich playas are the most likely terrestrial analog for the chloride-bearing terrains, which indicates extensive hydrological activity, although possibly transient, and may have required multiple recharging events by a near surface fluctuating water table to account for the salt–phyllosilicate associations.

3.3. PDPs in impact craters: crater-floor polygons (CFPs)

El-Maarry et al. (2010) used high resolution images from CTX, HiRISE and MOC images to map intermediate-sized (~100–200 m-wide) polygonal crack patterns in ~260 impact craters (Fig. 14). Whereas most of these features are concentrated in the high latitudes, their sizes are significantly larger than typical TCPs on Mars that tend to fall in the range of 5–20 m-wide (e.g., Levy et al., 2009; Fig. 14a). In addition, the distribution of features extends, albeit to a lesser degree, to the equator in both hemispheres. The patterns can fill the entire crater floor in the case of small craters (~20 km-wide or less) but may be restricted to certain locations or patches in larger impact craters or basins.
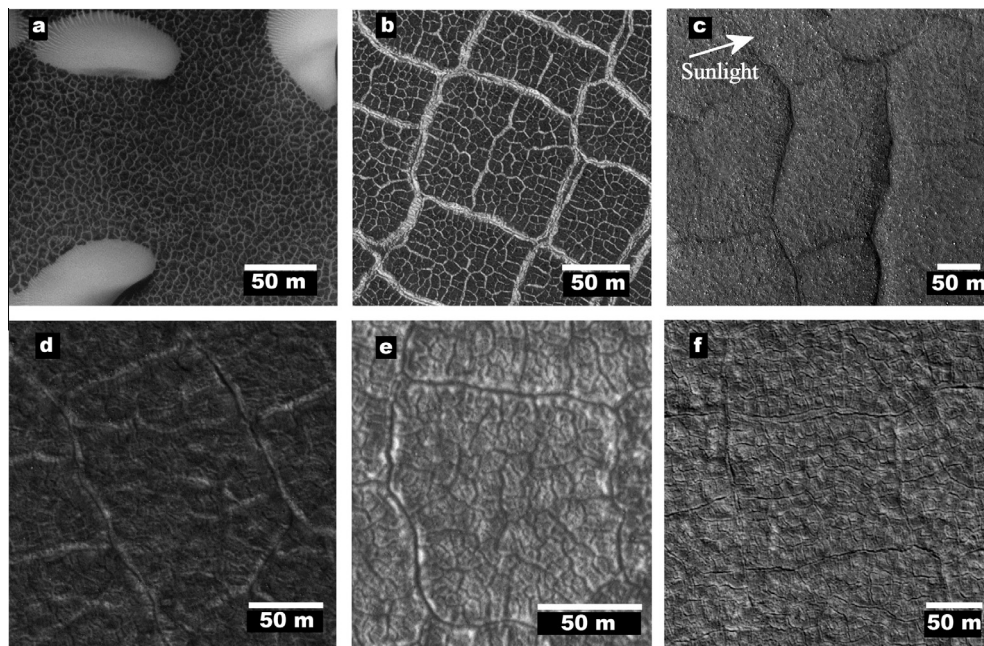
Fig. 14. Typical crater-floor polygons (CFPs) on Mars and comparison to thermal contraction polygons (TCPs). TCPs on Mars are typically 5–20 m wide and are ubiquitous in the high latitudes (a). CFPs, on the other hand, are usually associated with impact craters and range in size from 15 to 350 m. In the higher latitudes the fractures, usually 1– 10 m wide, are occasionally filled with frost or permanent ice (b) making it easier for visual detection as opposed to ice-free ones (e.g. c and f) and usually display two distinct size groups (b, d, e, and f): Large 70–350 m-sized polygons with an average polygon diameter of 120 m, and a smaller group, not always present, 5–20 m-wide, which are most likely TCPs. *Source*: HiRISE with image IDs: (a) PSP_008165_2505, (b) PSP_007372_2475, (c) PSP_001942_2310, (d) PSP_007573_2435, (e) PSP_008456_2460, and (f) PSP_010412_2475. Figure adapted from El-Maarry et al. (2012). Images credit: University of Arizona/JPL/NASA.

El-Maarry et al. (2010) used an analytical model based on fracture mechanics to show that TCPs can attain maximum sizes of ~25 m (~70 m in extreme and unusual cases) thereby making thermal contraction an improbable mechanism for the formation of CFPs– leaving desiccation as the more likely mechanism. Within this hypothesis, they suggested that craters displaying CFPs once harbored lakes (either open-systems or closed/hydrothermally generated) that have contributed to the formation of the CFPs. Many of such craters (~40%) show additional paleolake-indicators (El-Maarry et al., 2010) such as inlet/outlet channels, deltas, terraces, putative shorelines, mounds, and layered sediments (Cabrol and Grin, 1999). In addition, some of these craters show distinctive mineralogical signatures that suggest they hosted paleolakes.

Despite the collective evidence in support of desiccation, CFPs pose many questions that are yet to be addressed. For instance, many CFPs are located within Amazonian-aged impact craters (particularly in the high latitudes and the northern plains). Further studies are needed to investigate whether desiccation processes can take place in the current martian climatic setting. In addition, the preferential occurrence of CFPs in the high latitudes, while could be caused by observational biases (smaller areas mapped more densely, fractures filled with ice/frost easing detection, etc.), suggests that periglacial processes may also play a role in forming the CFPs.

3.4. In-situ observations by rovers

3.4.1. Opportunity rover at Meridiani

Both of the Mars Exploration Rovers (MER) encountered features that resemble desiccation polygons. By far the greatest variety and number were observed by the Opportunity rover at Meridiani Planum (Mclennan et al., 2005; Watters et al., 2011). The fractures are observed in light-toned aeolian sandstones composed of altered siliciclastic debris of basaltic composition (~40%)

as well as probable evaporites dominated by Mg-sulfates whose hydration state is not known (~50%) (McLennan et al., 2005). The sand-sized particles are thought to derive originally from evaporite-cemented basaltic muds (McLennan et al., 2005). In many locations, these rocks are covered by a <1 m layer of basaltic sand that commonly fills the fractures (Soderblom et al., 2004). Opportunity encountered widespread evidence of an ancient fluctuating water table and repeated episodes of wetting and drying associated with repeated dissolution, recrystallization and cementation of sulfate-rich sand grains and fracture walls (e.g., Grotzinger et al., 2005; McLennan et al., 2005; Knoll et al., 2008).

Small PDPs are ubiquitous at Meridiani Planum and occur in the following settings: (a) the walls of some impact craters, (b) boulders inside some impact craters (in float), (c) eroded ejecta blocks on the flanks of some craters, and (d) throughout the inter-crater plains. Fracture widths range from <1 mm to about 10 cm with spacing ranging from several mm to several meters. The widest and longest fractures at Meridiani occur in the plains, locally exhibit alignments and often do not connect to form classic shrinkage polygons (Watters et al., 2011, Fig. 15). Fracture networks with spacing at the meter scale and smaller are dominated by a hierarchical orthogonal pattern.

Unlike shrinkage fracturing that occurs at larger scales, small-scale fractures (<1 m spacing) sometimes also form "Y" junctions, with angles close to 120° instead of 90° (see Section 2.2). That is, it is not uncommon to observe a hierarchical pattern at larger scales and Y-junctions with pentagonal and hexagonal tiles only or primarily at the smallest scales (Fig. 15). The shrinkage-related fractures cut across bedding and are orthogonal to exposed surfaces rather than bedding in many boulders and rocks that have been displaced and rotated or exposed on crater walls (McLennan et al., 2005). In some cases, bedding has influenced the shape of polygonal tiles, creating a rectilinear pattern (Chan et al., 2008).

Multiple terrestrial analogs have been proposed for the Meridiani fractures, including thin (mm-scale) polygonal cracks in the
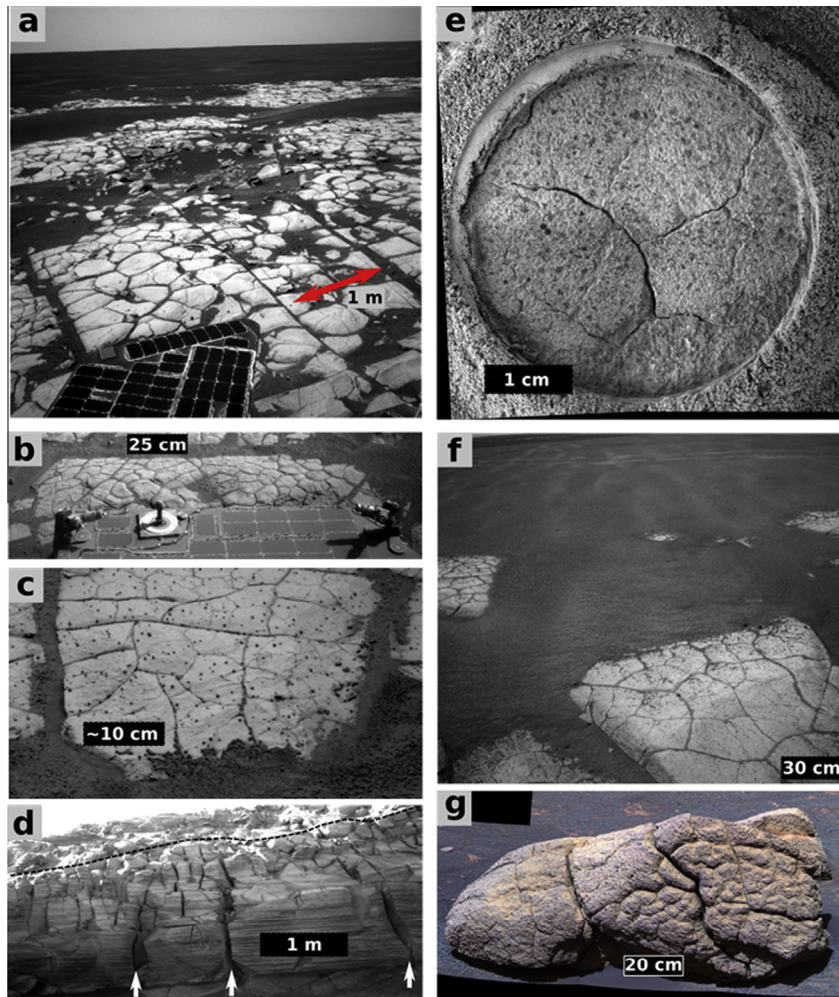
Fig. 15. Examples of shrinkage-related polygonal fracturing at Meridiani planum captured by the Opportunity rover. (a) Plains with meters-long fractures that exhibit regional alignments, as well as randomly-oriented fractures with orthogonal and Y junctions that exhibit sub-meter spacing (sol 649, Navcam 1N185802127EFF64EZP1700L0M1). (b) An example of small-scale tiles with orthogonal and Y junctions (sol 1806, Navcam 1N288519584EFF98J5P1925L0M1). (c) Example of dominantly hierarchical fracturing (sol 1934, Pancam 1P299873519EFFA3PGP2375R2M1) in a plains rock. (d) Cross-section of columnar shrinkage fractures in the eroded walls of Victoria crater (sol 1607 Navcam 1N270854057EFF90D8P0315L0M1). White arrows indicate position of widest fractures extending >2 m deep. Dashed line marks the pre-impact surface mantled by ejecta. (e) Microscopic imager mosaic of a rock surface with ~5 mm removed by the Rock Abrasion Tool (sol 894, sequence P2600), showing mm-scale orthogonal fractures. (f) Eroded ejecta blocks on the flanks of Victoria crater with primarily hierarchical shrinkage polygons (sol 1176, Navcam 1N232584064EFF82##P0623L0M1). (g) Densely-fractured meter-sized boulder "Wopmay" on sol 251 (false-color Pancam mosaic, sequence P2432) inside the 150 m-diameter Endurance crater. Images credit: JPL/NASA.

Navajo Sandstone (Chan et al., 2008), as well as cracks of a similar scale in weakly-cemented evaporite sands on dune slopes in the White Sands National Monument in New Mexico, USA (Chavdarian and Sumner, 2006, 2011). Both locations are dominated by Y-junction fractures that are shallower and narrower than all but the narrowest fractures at Meridiani. This implies that these terrestrial fractures and the processes that created them are relatively shallow (see Section 2.2). Rehydration and evaporation of a thin surface layer from frost or snow deposits is difficult to reconcile with the widest and deepest fractures at Meridiani. These fractures are more likely the consequence of shrinkage in a meters-thick stratum, such as may result from a subsiding water table. It is not known if the desiccation-related volume change is largely the outcome of mineral dehydration (e.g., of the sulfate-rich sand grains) or loss of pore fluid (McLennan et al., 2005).

3.4.2. Mars Science Laboratory at Gale crater

Shortly after the landing of the Mars Science Laboratory (MSL, also known as the Curiosity Rover) at Gale crater, a contact among three different geologic units, one with relatively high thermal inertia, was recognized within ~450 m of the landing spot, just

beyond the alluvial lobe of the Peace Vallis fan (Grotzinger et al., 2014). The decision to drive away from Mount Sharp toward this location, named the Yellow Knife Bay, has provided early samples of a mudstone that contains both clay minerals and sulfate salts (Vaniman et al., 2014). The samples (dubbed John Klein and Cumberland) were collected from the Sheepbed mudstone member of the sedimentary Yellowknife Bay formation, which is interpreted to be a shallow lacustrine deposit of Late Noachian to Early Hesperian age (Grotzinger et al., 2014).

HiRISE images reveal polygonal patterns (5–20 m-wide) on the surface of the geologic unit comprising the Yellowknife Bay formation, particularly to the northwest (Fig. 16). Moreover, the MSL rover observed small crack patterns forming generally <1 m-wide polygons that are likely formed by desiccation (Grotzinger et al., 2014, these should not be confused with similarly small polygonal ridges, nodules, and small fractures cross-cutting the aforementioned ridges, which are interpreted by the MSL team to be post-diagenetic features).

The John Klein and Cumberland samples contain tri-octahedral smectites (~20% by weight) along with detrital basaltic minerals, calcium sulfates (filling late diagenetic fractures), iron oxide or
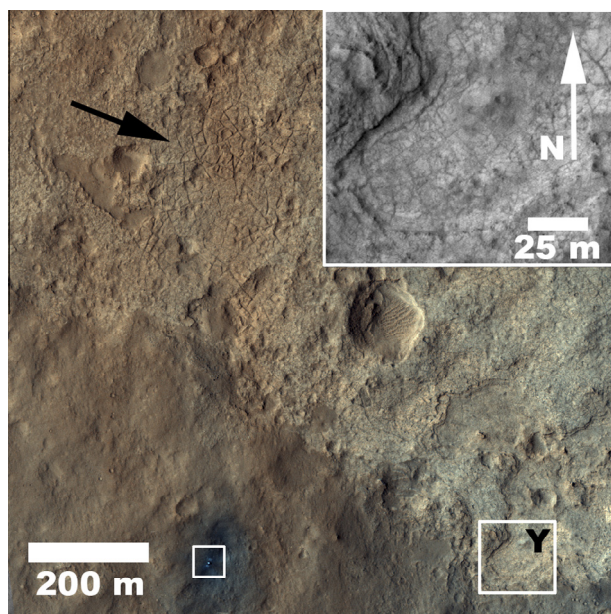
Fig. 16. HiRISE image ESP_028335_1755 in Gale crater showing the landing site of MSL along with the Rover shortly after landing (small white box). Approximately 450 m to the east, lies the Yellow Knife Bay (Y, large white box) where MSL collected two drill samples from a mudstone layer showing containing smectites (∼20 wt%) among other constituents. Also visible are polygonal patterns observed NW of Yellow Knife Bay (black arrow) but probably consisting of the same geological unit like Yellow Knife Bay. Inbox: Yellow Knife Bay area covered by the large white box in high spatial resolution using only the red filter of the same HiRISE image. Note the presence of 5-meters-wide PDPs. Image credit: University of Arizona/JPL/NASA.

hydroxides, iron sulfides, and amorphous material (Vaniman et al., 2014). The geometry of the fractures, the lack of a preferred fracture orientation, and the uniform size and shape of the intervening polygons suggest that they formed by contraction most probably related to desiccation or thermal contraction (Hallet et al., 2013).

4. Implications and outstanding questions

4.1. Identifying PDPs on Mars

The global distribution of PDPs shows that they share certain traits in terms of morphology and geologic setting that can aid in their identification and distinguish them from fracturing patterns caused by other processes (e.g., thermal contraction, tectonic, mechanical weathering, etc.). Morphologically, desiccation polygons can attain various shapes and sizes. More often than not, any single particular location will display fracturing patterns with a variable size range. Nonetheless, most PDPs currently observed from orbit attain a size range of 1–30 m-wide with the exception of the cm-sized polygons observed by rovers (Section 3.4) and the 100 + m-sized enigmatic CFPs that are observed inside impact craters (El-Maarry et al., 2010; Section 3.3). The variable size-range may suggest variable hydrologic conditions where small-sized polygons (10s–100s of cm-sized) may have formed through surface evaporation whereas larger ones (10s of meters) may suggest fluctuations in water-table level. Indeed, many of the regions discussed in Section 3.1 display various lines of evidence that suggest a hydrologically-active paleoenvironment. Moreover, many of the sites containing PDPs display clear phyllosilicate signatures in close association. Notably, PDPs are almost exclusively observed in light-toned units with respect to the surrounding terrain. They commonly underlie dark-toned materials, which are often spectrally featureless and display signs of recent exhumation.

Another key aspect in identifying PDPs, yet not exclusive to them, is the mode of intersection of the cracks, which tends to be orthogonal or quasi-orthogonal. The fracturing patterns tend to be more organized and attain intersection angles that are closest to 90° the larger the polygons get. This is to be expected because larger polygons tend to require more time to develop and imply a slowly-evolving stress system, which leads to sequential formation of cracks. Smaller polygons (5–10 m-wide) tend to be less regular and can be difficult to differentiate from irregular rock fractures or joints if they have been heavily degraded (Fig. 17). Desiccation polygons usually subdivide extensively to form secondary to multiple generations of cracks in a fractal-like pattern that is embedded within the larger primary polygons and requires images with sub-meter spatial resolution to identify. In addition, because of the slow buildup of stress, cracking tends to initiate by formation of a few long and sinuous cracks that ultimately intersect and create more subdivisions. Therefore, it is possible in some cases to identify the main fractures that initiate the pattern by their long sinuous nature and the fact that they tend to be the largest fractures in terms of length and width (see for example, the highlighted fractures in Fig. 7). Finally, PDPs do not usually possess raised rims or bulging centers that are common attributes of most classes of TCPs (Fig. 17a; Table 2). Instead, they usually form as flat patterns within sedimentary units with high brightness and albedo. It should be noted that this trait is not necessarily applicable to Earth since large desiccation polygons may progressively display raised rims because of preferential growth of vegetation in the polygons' troughs or re-expansion of the soil where moisture would concentrate seasonally (Neal et al., 1968).

In terms of regional and geologic setting, PDPs are expected to occur in regional depressions such as impact craters, or flat plains that may have harbored an aqueous environment at favorable climatic conditions. Therefore, PDPs are expected to concentrate in Noachian-aged (and probably Hesperian) terrains that show evidence of past liquid water activity. Common mineralogical associations are phyllosilicates, in particular smectites, sulfates, chlorides, and even carbonates. PDPs are not expected to form in volcanic terrains. Similarly, they are not expected to develop (at least in a size-scale visible from orbit) in most allogenic sediments or magmatic-/hydrothermally-derived deposits even if they were rich in the above-mentioned mineralogies. Indeed, the paucity of PDPs in terrains that display mineralogies indicative of formation in hydrothermal or generally elevated temperatures (e.g., Nili Fossae and hydrothermal units in northern circum-Hellas) supports these conclusions. Nonetheless, more research is needed to assess the viability of magmatic/hydrothermal clay minerals in exhibiting crack patterns. Therefore, PDPs can be a valuable aid in assessing the hydrological and geological history of a given site or the genesis of a given mineralogical assemblage. This role is discussed in the following section.

4.2. Desiccation polygons as markers of lacustrine environments

Lacustrine deposits are generally fine-grained sediments rich in clay minerals. Their high potential for concentrating and preserving organic compounds makes them prime targets for in-situ rover lander and rover missions that search for organic remnants of life on Mars (e.g., Ehlmann et al., 2008b; Summons et al., 2011; Bishop et al., 2013b). Therefore, it is important to develop new criteria for using remote sensing (orbital) data to help distinguish lacustrine environments from phyllosilicate-bearing strata that may have formed by other mechanisms such as fluvial, hydrothermal, aeolian or general metamorphic processes.

Previous studies dedicated to identifying ancient lakes on Mars have focused largely on the morphological evidence for lacustrine environments, including the identification of closed or open basins
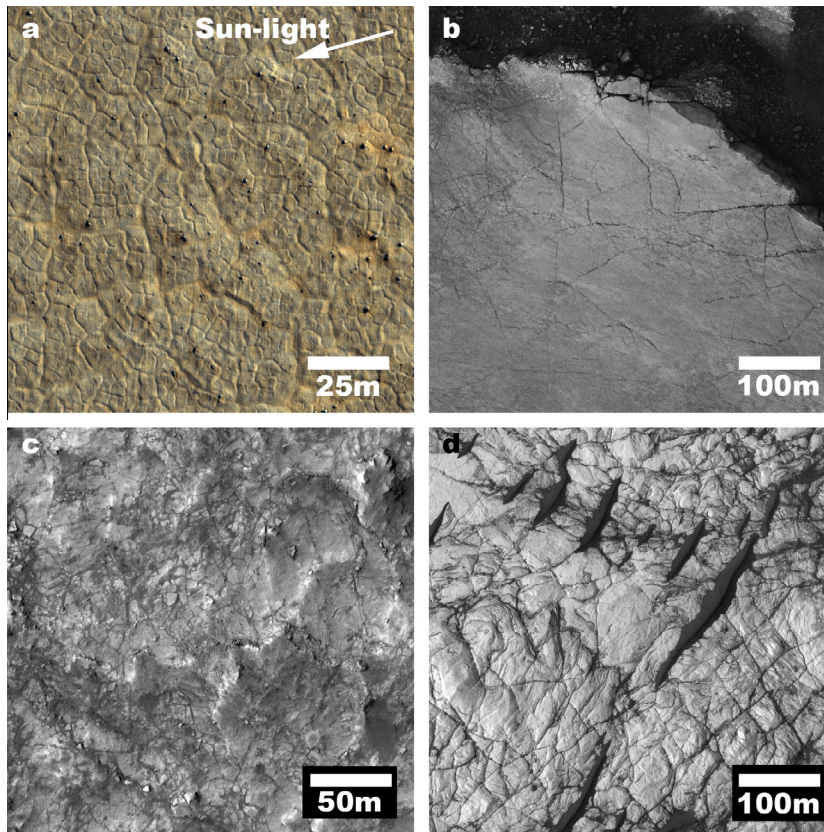
Fig. 17. HiRISE images of polygonal patterns on Mars that are not interpreted to be PDPs in this study. (a) High-latitude (70°N) polygonal patterns that are commonly identified as thermal contraction polygons (TCPs). Direction is sunlight is from the top right (arrow) and the image is taken at Ls 137 (northern summer). The rest: Polygonal patterns that are best explained by tectonic or mechanical weathering processes. In these localities, the polygonal patterns are not as organized as those of PDPs, the modes of intersection are irregular, the spectral analysis shows limited to absent signatures of hydrous minerals and the geologic setting does not indicate a paleolacustrine environment. In fact, the rocky unit in (d) has been proposed by Wray et al. (2013) to be granitic in composition, which could imply that the observed patterns are common granitic weathering joints. *Source*: Color and Red-filter HiRISE images with image IDs: (a) PSP_001474_2520, (b) PSP_003231_2095, (c) PSP_005764_1545, and (d) ESP_013504_1580. Images credit: University of Arizona/JPL/NASA.

with inlet (and outlet) channels, the presence of fan/deltaic features, terracing, and shoreline features just as examples (e.g., Cabrol and Grin, 1999, 2001; Grant and Parker, 2002; Fasset and Head, 2008). Later studies have attempted to develop mineralogical criteria (e.g., Bristow and Milliken, 2011; Ehlmann et al., 2011, 2013) to constrain the distribution of authigenic lacustrine clay minerals on Mars. In this respect, phyllosilicates exhibiting PDPs can act as a combined mineralogical and geomorphological criterion for the identification of lacustrine environments on Mars.

Unlike Earth, where Al-rich phyllosilicates dominate (Bristow and Milliken, 2011), Fe/Mg-rich varieties are the dominant clay minerals detected on Mars (e.g., Poulet et al., 2005; Murchie et al., 2009), which is generally attributed to the prevalence of basaltic material in the martian crust. Many of the authigenic clay minerals forming in terrestrial lakes are enriched in Mg, especially if they are formed under alkaline and/or saline conditions whereas nontronite rarely forms since other Fe-rich clays such as illite would tend to dominate. Nonetheless, the situation may have been different on Mars because of the higher iron contents. High delivery of iron oxides could act as nucleation sites for the formation of nontronite (Bristow and Milliken, 2011). Taking all this to consideration, we consider that, (1) detection of Fe/Mg smectites in a sedimentary setting (i.e., showing morphological signs like terracing, layering, shorelines, deltas, inlet/outlet channels, etc.) with salts, carbonates, kaolinite, and possibly illite (although admittedly rare on Mars), (2) absence of high temperature/pressure phases, and (3) association with polygonal patterns resembling PDPs, is a useful combination

of criteria for identification of paleolacustrine (and possibly pedogenic) environments on Mars. Whereas similar mineralogical assemblages can also be attributed to other formation mechanisms (e.g., Ehlmann et al., 2013), the presence of the polygonal crack patterns is a direct indication of considerable thickness of the fractured material (i.e. clay minerals-bearing deposits), which is more commonly associated with hydrous basin deposits that have been exposed by erosion as opposed to other mechanisms that create gradational/zonal, or selective alteration (e.g., in pores or veins).

4.3. The Noachian climate: contributing to the debate

The climatic conditions during the early history of Mars, the Noachian, is one of the most debated subjects in martian research (e.g., Fairén, 2010; Carr and Head, 2010; Head, 2013, and references therein). The extensive suite of geomorphological features (see Section 1) and associated mineralogies argue in favor of a more hydrologically active, and potentially warm, climate in the Noachian in comparison to the colder, more arid conditions, throughout the Amazonian. However, several studies challenge the early "warm and wet" Mars hypothesis (Head, 2013, and references therein). For instance, atmospheric modelers encounter difficulties in producing and maintaining an atmosphere that can sustain warm and wet pluvial conditions on early Mars as a result of the perceived faint young Sun during the Noachian and insufficient green-house gases (e.g., Haberle, 1998; Head, 2013). However, the "faint young Sun paradox" (Sagan and Mullen, 1972) is

Table 2
Comparison between PDPs and TCPs on Mars. See Section 4 for more detail.

Attribute	PDPs	TCPs on Mars
Morphology	Polygonal (4–6-sided) shapes created by intersection of tensile cracks	Same
Size-range	10^{-2}–10^2 m	5–25 m[a]
Crack intersections	Orthogonal to quasi-orthogonal. Patterns tend to become more ordered with size	Same
Cracking evolution	Subdivisions and multiple generations of cracks are common	Share the same attributes but more limited because of the constraints on evolution of thermal stresses controlled by thermal seasonal variations
Geologic setting	Fine-grained geological units in arid settings located in regional depressions and locations of ancient liquid water activity. Generally in the Noachian-aged southern highlands	Frozen soils in periglacial settings in association with other periglacial features or permafrost conditions. Generally in the mid- and high latitudes[b]
Associated mineralogical assemblage	Mainly associated with smectite authigenic clay-rich soils. Less commonly associated with other non-smectite clays (e.g., illite, kaolinite, etc.), sulfates and carbonates	Water–ice-rich soils of palagonetic (weathered basalt) composition

[a] According to global mapping studies and current climatic constraints on Mars (cf., Levy et al., 2009; Mellon, 1997; Mellon et al., 2008).

[b] The latitudinal trend is generally applicable only to recent TCPs. Mars has experienced numerous obliquity changes over the past >3 Gyr (Laskar et al., 2004), causing major shifts in the equatorial/pole positions. Therefore, it is possible that some (likely highly degraded) relict TCPs may yet be observable in lower latitudes.

also applicable to Earth where there is extensive evidence for warm conditions on Earth during that period (e.g., Craddock et al., 2013). Other studies suggest a thin Noachian atmosphere that was unable to sustain warm conditions based on studies of martian meteorites (Cassata et al., 2012) while others derive lower estimates of water lost to space than previously thought, which challenges the hypothesis of a previously thick Noachian atmosphere being lost to space (Chassefière and Leblanc, 2011).

Many recent studies suggest different pathways in which hydrologically-formed features may evolve in cold and arid climatic settings similar to the current conditions. For example, Ehlmann et al. (2011) suggest that many of the martian phyllosilicates, in particular those in association with chlorites and high-temperature phases such as prehnite, have actually formed through hydrothermal (subsurface) alteration. Field studies in the Antarctic Dry Valleys show that meltwater-related fluvial activity can occur even when mean annual temperatures are below freezing (Marchant and Head, 2007) while modeling studies show the feasibility of liquid water activity at subzero temperatures as long as the water solutions contain enough freezing-point depressing solutes (e.g., Fairén, 2010). Finally, punctuated volcanic activity could lead to transient atmospheric warming and extensive melting of surface ice in a predominantly cold early Mars (Halevy and Head, 2012).

The presence of PDPs in association with many phyllosilicate exposures that are located in natural basins and/or are of sedimentary origin argues for a more hydrologically active period and warmer conditions than what is observed today. However, the presence of desiccation polygons is similarly consistent with climatic conditions that display only short intermittent hydrological activity characterized by ground-water activity in generally arid conditions. In fact, many of the sites containing PDPs, in particular those in association with chlorides, are indicative of multiple ground-water recharging and water-table fluctuations (Section 3.2 and references therein). More experimental and modeling work is needed, and currently in progress (e.g., El-Maarry et al., 2013b) to better understand the constraints on desiccation in various martian climatic conditions. In addition, a detailed analysis of the timing of formation of phyllosilicate-bearing deposits that display PDPs may help constrain the period(s) of hydrological activity during the Noachian and the Noachian/Hesperian transition.

5. Summary and conclusions

We have presented here a synthesis of the collective evidence that shows that desiccation cracks maybe more common on the surface of Mars than previously thought. The state of terrestrial research on desiccation processes has also been reviewed with emphasis on the theoretical background, field studies, and modeling constraints.

Potential desiccation polygons (PDPs) are a common feature in phyllosilicate- and chloride-bearing terrains and have been observed with size scales that range from cm- to 10s of meters-wide using images from HiRISE and currently active rovers. The global distribution of PDPs shows that they share certain traits in terms of morphology and geologic setting that can aid in their identification and distinguish them from fracturing patterns caused by other processes. Most PDPs currently observed from orbit attain a size range of 1–30 m-wide. PDPs are almost exclusively observed in light-toned units with respect to the surrounding terrain. They are generally flat (lacking raised rims or bulging centers) and usually subdivide extensively to form secondary to multiple generations of cracks in a fractal-like pattern that is embedded within the larger primary polygons and requires images with sub-meter spatial resolution to identify. PDPs are mostly associated with sedimentary deposits that display spectral evidence for the presence of Fe/Mg smectites or vermiculites in addition to Al-rich smectites and less commonly kaolinites and carbonates. In contrast, PDPs are uncommon in materials that have been heavily modified by erosion, tectonism, or extensive reworking (e.g., central-peak materials uplifted by impact cratering). Similarly, they are uncommon in materials of possible geothermal or hydrothermal origin, which is inferred from the presence of high-temperature or pressure mineral phases such chlorites, prehnite and serpentine.

PDPs observed from orbit can be excellent markers for paleolacustrine environments and their presence implies that the fractured units are rich in smectite minerals. Together, the following criteria: (1) detection of Fe/Mg smectites in a sedimentary setting along with salts, carbonates, kaolinite, and possibly illite, (2) absence of high temperature/pressure phases, and (3) association with polygonal patterns resembling PDPs make a certain location a high candidate for a paleolacustrine site on Mars, which is a top-priority setting for in-situ exploration and search for paleo-organic materials. The presence of desiccation features in association with many phyllosilicate exposures that are located in natural basins and/or are of sedimentary origin would argue for a more hydrologically active period and warmer conditions than what is observed today. However, the presence of desiccation polygons is similarly consistent with climatic conditions that display only short intermittent hydrological activity characterized by ground-water activity in generally arid conditions.

Acknowledgments

Appendix A. Supplementary material

Supplementary data associated with this article can be found, in the online version, at http://dx.doi.org/10.1016/j.icarus.2014.06.033.

References

Amarasiri, A.L., Kodikara, J.K., Costa, S., 2010. Numerical modeling of desiccation cracking. Int. J. Numer. Anal. Geomech, doi:10.1002/nag.894.

Anderson, R.C. et al., 2001. Significant centers of tectonic activity through time for the western hemisphere of Mars. J. Geophys. Res. 106, 20563–20585.

Baker, V.R., 2001. Water and the martian landscape. Nature 412, 228–356.

Baker, V.R., Strom, R.G., Gulick, V.C., Kargel, J.S., Komatsu, G., 1991. Ancient oceans, ice sheets and the hydrological cycle on Mars. Nature 352, 589–594.

Baria, L.R., 1977. Desiccation features and the reconstruction of paleosalinities. J. Sediment. Petrol. 47 (2), 908–914.

Bibring, J.-P. et al., 2004. OMEGA: Observatoire pour la Minéralogie, l'Eau, les Glaces et l'Activité. Eur. Space Agency Spec. Publ., ESA SP-1240, pp. 37–49.

Bibring, J.-P. et al., 2005. Mars surface diversity as revealed by the OMEGA/Mars Express Observations. Science 307, 1576–1581.

Bibring, J.-P. et al., 2006. Global mineralogical and aqueous Mars history derived from OMEGA/Mars Express data. Science 312, 400–404. http://dx.doi.org/10.1126/science.1122659.

Bishop, J.L. et al., 2008. Phyllosilicate diversity and past aqueous activity revealed at Mawrth Vallis, Mars. Science 321, 830–833.

Bishop, J.L. et al., 2013a. Mineralogy and morphology of geologic units at Libya Montes, Mars: Ancient aqueously derived outcrops, mafic flows, fluvial features, and impacts. J. Geophys. Res.: Planets 118, 487–513. http://dx.doi.org/10.1029/2012JE004151.

Bishop, J.L. et al., 2013b. What the ancient phyllosilicates at Mawrth Vallis can tell us about possible habitability on early Mars. Planet. Space Sci. 86, 130–149.

Blasius, K.R., Cutts, J.A., 1981. Topography of martian central volcanoes. Icarus 45, 87–112.

Boynton, W.V. et al., 2007. Concentration of H, Si, Cl, K, Fe, and Th in the low and mid latitude regions of Mars. J. Geophys. Res. 112, E12S99. http://dx.doi.org/10.1029/2007JE002887.

Bristow, T., Milliken, R.E., 2011. Terrestrial perspective on authigenic clay mineral production in ancient martian lakes. Clays Clay Miner. 59 (4), 339–358.

Brown, A.J. et al., 2010. Hydrothermal formation of clay-carbonate alteration assemblages in the Nili Fossae region of Mars. Earth Planet. Sci. Lett. 297, 174–182.

Cabrol, N.A., Grin, E.A., 1999. Distribution, classification, and ages of martian impact crater lakes. Icarus 142, 160–172.

Cabrol, N.A., Grin, E.A., 2001. The evolution of Lacustrine environments on Mars: Is Mars only hydrologically dormant? Icarus 149, 291–328.

Carr, M.H., 1986. Mars – A water-rich planet? Icarus 68, 187–216.

Carr, M.H., 1995. The martian drainage system and the origin of valley networks and fretted channels. J. Geophys. Res. 100 (E4), 7479–7507. http://dx.doi.org/10.1029/95JE00260.

Carr, M.H., 1996. Water on Mars. Oxford University Press, New York, 248p.

Carr, M.H., Head, J.W., 2010. Geologic history of Mars. Earth Planet. Sci. Lett. 294, 185–203.

Carter, J., Poulet, F., Bibring, J.-P., Murchie, S., 2010. Detection of hydrated silicates in crustal outcrops in the northern plains of Mars. Science 328, 1682–1686.

Carter, J., Poulet, F., Bibring, J.-P., Mangold, N., Murchie, S., 2013. Hydrous minerals on Mars as seen by the CRISM and OMEGA imaging spectrometers: Updated global view. J. Geophys. Res.: Planets 118, 831–858. http://dx.doi.org/10.1029/2012JE004145.

Cassata, W.S., Shuster, D.L., Renne, P.R., Weiss, B.P., 2012. Trapped Ar isotopes in meteorite ALH 84001 indicate Mars did not have a thick ancient atmosphere. Icarus 221, 461–465.

Chan, M.A., Yonkee, W.A., Netoff, D.I., Seiler, W.M., Ford, R.L., 2008. Polygonal cracks in bedrock on Earth and Mars: Implications for weathering. Icarus 194, 65–71. http://dx.doi.org/10.1016/j.icarus.2007.09.026.

Chassefière, E., Leblanc, F., 2011. Constraining methane release due to serpentinization by the D/H ratio on Mars. Earth Planet. Sci. Lett. 310, 262–271.

Chavdarian, G.V., Sumner, D.Y., 2006. Cracks and fins in sulfate sand: Evidence for recent mineral–atmospheric water cycling in Meridiani outcrops? Geology 34, 229–232. http://dx.doi.org/10.1130/G22101.1.

Chavdarian, G.V., Sumner, D.Y., 2011. Origin and evolution of polygonal cracks in hydrous sulphate sands, White Sands National Monument, New Mexico. Sedimentology 58, 407–423. http://dx.doi.org/10.1111/j.1365-3091.2010.01169.x.

Christensen, P.R. et al., 2001. Mars Global Surveyor Thermal Emission Spectrometer experiment: Investigation description and surface science results. J. Geophys. Res. 106 (E10), 23823–23872.

Christensen, P.R. et al., 2004. The THermal Emission Imaging System (THEMIS) for the Mars 2001 Odyssey mission. Space Sci. Rev. 110, 85–130.

Corte, A., Higashi, A., 1964. Experimental research on desiccation cracks in soil. CRREL Res. Rep., 66. U.S. Army Material Command, Hanover, NH.

Costanzo, P.M., Guggenheim, S., 2001. Baseline studies of the clay minerals society source clays: Preface. Clays Clay Miner. 49, 371.

Craddock, R.A., Irwin, R.P., Howard, A.D., Latham, D.W., 2013. The history of water on early Mars: The Sun, the wind, and the rain. Lunar Planet. Sci. Abstract #1984.

Crumpler, L.S., Tanaka, K.L., 2003. Geology and MER target site characteristics along the southern rim of Isidis Planitia, Mars. J. Geophys. Res. 108, 8080. http://dx.doi.org/10.1029/2002JE002040, E12.

Davila, A.F., Gross, C., Marzo, G.A., Fairen, A.G., Kneissl, T., McKay, C.P., Dohm, J.M., 2010. A large sedimentary basin in the Terra Sirenum region of the southern highlands of Mars. Icarus 212, 579–589.

Di Achille, G., Hynek, B.M., 2010. Ancient ocean on Mars supported by global distribution of deltas and valleys. Nat. Geosci. 3, 459–463.

Di Achille, G., Ori, G., Reiss, D., 2007. Evidence for Late Hesperian lacustrine activity in Shalbatana Vallis, Mars. J. Geophys. Res. 112, E07007.

Di Achille, G., Hynek, B.M., Searls, M.L., 2009. Positive identification of lake strandlines in Shalbatana Vallis, Mars. Geophys. Res. Lett. 36, L14201.

Dohm, J.M. et al., 2001. Ancient drainage basin of the Tharsis region, Mars: Potential source for outflow channel systems and putative oceans or paleolakes. J. Geophys. Res. 106, 32943–32958.

Domenico, P.A., Schwartz, F.W., 1998. Physical and Chemical Hydrogeology, second ed. John Wiley & Sons.

Ehlmann, B.L. et al., 2008a. Orbital identification of carbonate-bearing rocks on Mars. Science 322, 1828–1832.

Ehlmann, B.L. et al., 2008b. Clay minerals in delta deposits and organic preservation potential on Mars. Nat. Geosci. 1, 355–358.

Ehlmann, B.L. et al., 2009. Identification of hydrated silicate minerals on Mars using MRO-CRISM: Geologic context near Nili Fossae and implications for aqueous alteration. J. Geophys. Res. 114, E00D08. http://dx.doi.org/10.1029/2009JE003339.

Ehlmann, B.L., Mustard, J.F., Murchie, S.L., 2010. Geologic setting of serpentine deposits on Mars. Geophys. Res. Lett. 37, L06201. http://dx.doi.org/10.1029/2010GL042596.

Ehlmann, B.L. et al., 2011. Subsurface water and clay mineral formation during the early history of Mars. Nature 479, 53–60.

Ehlmann, B.L. et al., 2013. Geochemical consequences of widespread clay mineral formation in Mars' ancient crust. Space Sci. Rev. 174 (1–4), 329–364.

El-Maarry, M.R., Markiewicz, W.J., Mellon, M.T., Goetz, W., Dohm, J.M., Pack, A., 2010. Crater floor polygons: Desiccation patterns of ancient lakes? J. Geophys. Res. 115, E10006. http://dx.doi.org/10.1029/2010JE003609.

El-Maarry, M.R., Kodikara, J., Wijessoriya, S., Markiewicz, W.J., Thomas, N., 2012. Desiccation mechanism for formation of giant polygons on Earth and intermediate-sized polygons on Mars: Results from a pre-fracture model. Earth Planet. Sci. Lett. 323, 19–26.

El-Maarry, M.R., Pommerol, A., Thomas, N., 2013a. Analysis of polygonal cracking patterns in chloride-bearing terrains on Mars: Indicators of ancient playa settings. J. Geophys. Res.: Planets 118. http://dx.doi.org/10.1002/2013JE004463.

El-Maarry, M.R., Pommerol, A., Thomas, N., 2013b. Desiccation experiments using wet clay bearing soils as an analogue for desiccation cracks on Mars. In: Europlanet Science Conference. Abstract #447.

Erkeling, G., Reiss, D., Hiesinger, H., Jaumann, R., 2010. Morphologic, stratigraphic and morphometric investigations of valley networks in eastern Libya Montes, Mars: Implications for the Noachian/Hesperian climate change. Earth Planet. Sci. Lett. 294, 291–305.

Erkeling, G. et al., 2012. Valleys, paleolakes and possible shorelines at the Libya Montes/Isidis boundary: Implications for the hydrologic evolution of Mars. Icarus 219, 393–413.

Fairén, A.G., 2010. A cold and wet Mars. Icarus 208, 165–175.

Farrand, W.H., Glotch, T.D., Rice Jr., J.W., Hurowitz, J.A., Swayze, G.A., 2009. Discovery of jarosite within the Mawrth Vallis region of Mars: Implications for the geologic history of the region. Icarus 204 (2), 478–488.

Fasset, C.I., Head, J.W., 2008. The timing of martian valley network activity: Constraints from buffered crater counting. Icarus 195, 61–89.

Fisher, D.A., 2005. A process to make massive ice in the martian regolith using long-term diffusion and thermal cracking. Icarus 179, 387–397.

Glotch, T.D., Bandfield, J.L., Tornabene, L.L., Jensen, H.B., Seelos, F.P., 2010. Distribution and formation of chlorides and phyllosilicates in Terra Sirenum, Mars. Geophys. Res. Lett. 37, L16202.

Goehring, L., 2009. Drying and cracking mechanisms in a starch slurry. Phys. Rev. E 80, 036116.

Goehring, L., 2013. Evolving fracture patterns: Columnar joints, mud cracks, and polygonal terrain. Philos. Trans. R. Soc. A 371, 20120353.

Goehring, L., Conroy, R., Akhter, A., Clegg, W.J., Routh, A.F., 2010. Evolution of mud-crack patterns during repeated drying cycles. Soft Matter 6, 3562–3567.

Golombek, M. et al., 2012. Selection of the Mars Science Laboratory landing site. Space Sci. Rev., 1–97.

Grant, J.A., Parker, T.J., 2002. Drainage evolution in the Margaritifer Sinus region, Mars. J. Geophys. Res. 107 (E9), 5066. http://dx.doi.org/10.1029/2001JE001678.

Grant, J.A., Schultz, P.H., 1990. Gradational epochs on Mars – Evidence from west–northwest of Isidis Basin and Electris. Icarus 84, 166–195.

Grant, J.A., Wilson, S.A., Noe Dobrea, E., Fergason, R.L., Griffes, J.L., Moore, J.M., Howard, A.D., 2010. HiRISE views enigmatic deposits in the Sirenum Fossae region of Mars. Icarus 205 (1), 53–63.

Grindrod, P.M., West, M., Warner, N.H., Gupta, S., 2012. Formation of an Hesperian aged sedimentary basin containing phyllosilicates in Coprates Catena, Mars. Icarus 218, 178–195.

Grotzinger, J.P. et al., 2005. Stratigraphy and sedimentology of a dry to wet eolian depositional system, Burns formation, Meridiani Planum, Mars. Earth Planet. Sci. Lett. 240, 11–72. http://dx.doi.org/10.1016/j.epsl.2005.09.039.

Grotzinger, J.P. et al., 2014. A habitable fluvio-lacustrine environment at Yellowknife Bay, Gale crater, Mars. Science 343 (6169). http://dx.doi.org/10.1126/science.1242777.

Gulick, V., 2001. Origin of the valley networks on Mars: A hydrological perspective. Geomorphology 37, 241–268.

Haberle, R.M., 1998. Early Mars climate models. J. Geophys. Res. 103, 28467–28480.

Halevy, I., Head, J.W., 2012. Climatic effects of punctuated volcanism on early Mars. LPI Contributions 1680, 7043.

Hallet, B. et al., 2013. Fracture networks, Gale crater, Mars. Lunar Planet. Sci. XXIV. Abstract #3108.

Harris, R.C., 2004. Giant Desiccation Cracks in Arizona. Arizona Geological Survey Open File Report, OFR-04-01, 93 p.

Hartmann, W.K., Neukum, G., 2001. Cratering chronology and the evolution of Mars. Space Sci. Rev. 96, 165–194.

Head, J., 2013. The early climate history of Mars: "Warm and wet" or "cold and dry"? Lunar Planet. Sci. Abstract #1523.

Hoefen, T.M., Clark, R.N., Bandfield, J.L., Smith, M.D., Pearl, J.C., Christensen, P.R., 2003. Discovery of olivine in the Nili Fossae region of Mars. Science 302, 627–630.

Howard, A.D., Moore, J.M., 2004. Scarp-bounded benches in Gorgonum Chaos, Mars: Formed beneath an ice-covered lake? Geophys. Res. Lett. 31 (1), L01702.

Hu, L.B., Péron, H., Hueckel, T., Laloui, L., 2006. Numerical and phenomenological study of desiccation of soil. In: Advances in Unsaturated Soil, Seepage and Environmental. ASCE Geotechnical Special Publication, 2006, pp. 166–173.

Hynek, B.M., Phillips, R.J., Arvidson, R.E., 2003. Explosive volcanism in the Tharsis region: Global evidence in the martian geologic record. J. Geophys. Res. 108, 5111. http://dx.doi.org/10.1029/2003JE002062, E9.

Hynek, B.M., Beach, M., Hoke, M.R.T., 2010. Updated global map of martian valley networks and implications for climate and hydrologic processes. J. Geophys. Res. 115, E09008. http://dx.doi.org/10.1029/2009JE003548.

Irwin III, R.P., Howard, A.D., Maxwell, T.A., 2004. Geomorphology of Ma'adim Vallis, Mars, and associated paleolake basins. J. Geophys. Res. 109 (E12), E12009.

Jagla, E.A., 2004. Maturation of crack patterns. Phys. Rev. E 69, 056212.

Jaumann, R., Nass, A., Tirsch, D., Reiss, D., Neukum, G., 2010. The western Libya Montes valley system on Mars: Evidence for episodic and multi-genetic erosion events during the martian history. Earth Planet. Sci. Lett. 294, 272–290.

Karunatillake, S. et al., 2007. Chemical compositions at Mars landing sites subject to Mars Odyssey Gamma Ray Spectrometer constraints. J. Geophys. Res. 112, E08S90. http://dx.doi.org/10.1029/2006JE002859.

Kerber, L., Head, J.W., Madeleine, J.-B., Forget, F., Wilson, L., 2012. The dispersal of pyroclasts from ancient explosive volcanoes on Mars: Implications for the friable layered deposits. Icarus 219, 358–381.

Knoll, A.H. et al., 2008. Veneers, rinds, and fracture fills: Relatively late alteration of sedimentary rocks at Meridiani Planum, Mars. J. Geophys. Res.: Planets 113, E06S16. http://dx.doi.org/10.1029/2007JE002949.

Kodikara, J.K., Nahlawi, H., Bouazza, A., 2004. Modeling of curling in desiccating clay. Can. Geotech. J. 41, 560–566.

Konrad, J.M., Ayad, R., 1997. An idealized framework for the analysis of cohesive soils undergoing desiccation. Can. Geotech. J. 34, 477–488.

Lachenbruch, A.H., 1961. Depth and spacing of tension cracks. J. Geophys. Res. 66 (12), 4273–4292.

Lachenbruch, A.H., 1962. Mechanics of thermal contraction cracks and ice-wedge polygons in permafrost. Spec. Pap. Geological society of America, 70. 69pp.

Langevin, Y., Poulet, F., Bibring, J.-P., Gondet, B., 2005. Sulfates in the north polar region of Mars detected by OMEGA/Mars Express. Science 307, 1584–1586.

Laskar, J., Correia, A.C.M., Gastineau, M., Joutel, F., Levrard, B., Robutel, P., 2004. Long term evolution and chaotic diffusion of isolation quantities of Mars. Icarus 170, 343–364.

Lawrence, A.H., Smoot, J.P., Eugster, H.P., 1978. Saline lakes and their deposits: A sedimentological approach. Spec. Publs. Int. Ass. Sediment. 2, 7–41.

Le Deit, L. et al., 2012. Extensive surface pedogenic alteration of the martian Noachian crust suggested by plateau phyllosilicates around Valles Marineris. J. Geophys. Res. 117, E00J05. http://dx.doi.org/10.1029/2011JE003983.

Lefort, A., Russell, P.S., Thomas, N., 2010. Scalloped terrains in the Peneus and Amphitrites Paterae region of Mars as observed by HiRISE. Icarus 205, 259–268.

Leonard, G.J., Tanaka, K.L., 2001. Geologic Map of the Hellas Region of Mars. US-Geological Survey Map I-2694.

Levy, J., Head, J.W., Marchant, D., 2009. Thermal contraction crack polygons on Mars: Classification, distribution, and climate implications from HiRISE

observations. J. Geophys. Res. 114, E01007. http://dx.doi.org/10.1029/2008JE003273.

Loizeau, D. et al., 2007. Phyllosilicates in the Mawrth Vallis region of Mars. J. Geophys. Res. 112, E08S08. http://dx.doi.org/10.1029/2006JE002877.

Loizeau, D. et al., 2010. Stratigraphy in the Mawrth Vallis region through OMEGA. HRSC color imagery and DTM. Icarus 205 (2), 396–418.

Loizeau, D., Werner, S.C., Mangold, N., Bibring, J.-P., Vago, J.L., 2012. Chronology of deposition and alteration in the Mawrth Vallis region, Mars. Planet. Space Sci. 72, 31–43.

Loope, D.B., Haverland, Z.E., 1988. Giant desiccation fissures filled with calcareous eolian sand, Hermosa Formation (Pennsylvanian), southern Utah. Sediment. Geol. 56, 403–413.

Lucchitta, B.K., 1981. Mars and Earth: Comparison of cold-climate features. Icarus 45, 264–303.

Maloof, A.C., Kellogg, J.B., Anders, A.M., 2002. Neoproterozoic sand wedges: Crack formation in frozen soils under diurnal forcing during a snowball Earth. Earth Planet. Sci. Lett. 204 (1–2), 1–15. http://dx.doi.org/10.1016/S0012-821X(02)00960-3.

Mangold, N., 2005. High latitude patterned ground on Mars: Classification, distribution and climatic control. Icarus 174, 336–359.

Mangold, N. et al., 2007. Mineralogy of the Nili Fossae region with OMEGA/Mars Express data: 2. Aqueous alteration of the crust. J. Geophys. Res. 112, E08S04. http://dx.doi.org/10.1029/2006JE002835.

Mangold, N. et al., 2008. Spectral and geological study of the sulfate-rich region of West Candor Chasma, Mars. Icarus 194, 519–543.

Marchant, D.R., Head, J.W., 2007. Antarctic dry valleys: Microclimate zonation, variable geomorphic processes, and implications for assessing climate change on Mars. Icarus 192, 187–222.

McEwen, A.S. et al., 2007. Mars Reconnaissance Orbiter's High Resolution Imaging Science Experiment (HiRISE). J. Geophys. Res. 112, E05S02. http://dx.doi.org/10.1029/2005JE002605.

McGill, G.E., Hills, L.S., 1992. Origin of giant martian polygons. J. Geophys. Res.: Planets 97, 2633–2647. http://dx.doi.org/10.1029/91JE02863.

McKeown, N.K. et al., 2009. Characterization of phyllosilicates observed in the central Mawrth Vallis region, Mars, their potential formational processes, and implications for past climate. J. Geophys. Res. 114, E00D10. http://dx.doi.org/10.1029/2008JE003301.

McKeown, N.K. et al., 2011. Interpretation of reflectance spectra of clay mineral–silica mixtures: Implications for martian clay mineralogy at Mawrth Vallis. Clays Clay Miner. 59 (4), 400–415.

McKeown, N.K., Bishop, J.L., Silver, E.A., 2013. Variability of rock texture and morphology correlated with the clay-bearing units at Mawrth Vallis, Mars. J. Geophys. Res.: Planets 118, 1245–1256. http://dx.doi.org/10.1002/jgre.20096.

McLennan, S.M. et al., 2005. Provenance and diagenesis of the evaporite-bearing Burns formation, Meridiani Planum, Mars. Earth Planet. Sci. Lett. 240, 95–121. http://dx.doi.org/10.1016/j.epsl.2005.09.041.

Mellon, M.T., 1997. Small-scale polygonal features on Mars: Seasonal thermal contraction cracks in permafrost. J. Geophys. Res. 102 (E11), 25617–25628. http://dx.doi.org/10.1029/97JE02582.

Mellon, M.T., Arvidson, R.E., Marlow, J.J., Phillips, R.J., Asphaug, E., 2008. Periglacial landforms at the Phoenix landing site and the northern plains of Mars. J. Geophys. Res. 113, E00A23. http://dx.doi.org/10.1029/2007JE003039.

Mellon, M.T. et al., 2009. Ground ice at the Phoenix landing site: Stability state and origin. J. Geophys. Res. 114, E00E07. http://dx.doi.org/10.1029/2009JE003417.

Moscardelli, L., Dooley, T., Dunlap, D., Jackson, M., Wood, L., 2012. Deepwater polygonal fault systems as terrestrial analogs for large-scale martian polygonal terrains. GSA Today 22 (8), 4–9.

Müller, G., 1998. Starch columns: Analog model for basalt columns. J. Geophys. Res. 103, 15239–15253. http://dx.doi.org/10.1029/98JB00389.

Murchie, S. et al., 2007. Compact Reconnaissance Imaging Spectrometer for Mars (CRISM) on Mars Reconnaissance Orbiter (MRO). J. Geophys. Res. 112, E05S03. http://dx.doi.org/10.1029/2006JE002682.

Murchie, S.L. et al., 2009. A synthesis of martian aqueous mineralogy after 1 Mars year of observations from the Mars Reconnaissance Orbiter. J. Geophys. Res. 114, E00D06. http://dx.doi.org/10.1029/2009JE003342.

Mustard, J.F. et al., 2005. Olivine and pyroxene diversity in the crust of Mars. Science 307, 1587–1591.

Mustard, J.F. et al., 2007. Mineralogy of the Nili Fossae region with OMEGA/Mars Express data: 1. Ancient impact melt in the Isidis Basin and implications for the transition from Noachian to Hesperian. J. Geophys. Res. 112. http://dx.doi.org/10.1029/2006JE002834.

Mustard, J.F. et al., 2009. Hydrated silicate minerals on Mars observed by the Mars Reconnaissance Orbiter CRISM instrument. Nature 454, 305–309.

Mutch, T.A. et al., 1976. The surface of Mars: The view from the Viking 2 Lander. Science 194, 1277–1283. http://dx.doi.org/10.1126/science.194.4271.1277.

Nahalawi, H., Kodikara, J.K., 2006. Laboratory experiments on desiccation cracking of thin soil layers. Geotech. Geol. Eng. 24, 1641–1664.

Neal, J.T., Langer, A.M., Kerr, P.F., 1968. Giant desiccation polygons of Great Basin Playas. Geol. Soc. Am. Bull. 79, 69–90.

Noe Dobrea, E.Z., Swayze, G.A., 2012. Hydrothermal alteration products in the circum-Hellas region: Targets for future landed missions. Lunar Planet. Sci. 43. Abstract #1009.

Noe Dobrea, E.Z. et al., 2010. Mineralogy and stratigraphy of phyllosilicate-bearing and dark mantling units in the greater Mawrth Vallis/West Arabia terra area: Constraints on geological origin. J. Geophys. Res.: Planets 115, E00D19. http://dx.doi.org/10.1029/2009JE003351.

Noe Dobrea, E.Z., Michalski, J., Swayze, G., 2011. Aqueous mineralogy and stratigraphy at and around the proposed Mawrth Vallis MSL Landing Site: New insights into the aqueous history of the region. Mars 6, 32–46. http://dx.doi.org/10.1555/mars.2011.0003.

Osterloo, M.M. et al., 2008. Chloride-bearing materials in the southern highlands of Mars. Science 319, 1651–1654. http://dx.doi.org/10.1126/science.1150690.

Osterloo, M.M., Anderson, F.S., Hamilton, V.E., Hynek, B.M., 2010. Geologic context of proposed chloride-bearing materials on Mars. J. Geophys. Res. 115, E10012. http://dx.doi.org/10.1029/2010JE003613.

Parker, A.P., 1999. Stability of arrays of multiple edge cracks. Eng. Fract. Mech. 62 (6), 577–591.

Pechmann, J.C., 1980. The origin of polygonal troughs on the northern plains of Mars. Icarus 42, 185–210. http://dx.doi.org/10.1016/0019-1035(80)90071-8.

Peron, H., Delenne, J.Y., Laloui, L., El Youssoufi, M.S., 2009a. Discrete element modeling of drying shrinkage and cracking of soils. Comput. Geotech. 36, 61–69.

Peron, H., Hueckel, T., Laloui, L., Hu, L.B., 2009b. Fundamentals of desiccation cracking of fine-grained soil: Experimental characterization and mechanisms identification. Can. Geotech. J. 46, 1177–1201.

Plummer, P.S., Gostin, V.A., 1981. Shrinkage cracks: Desiccation or synaeresis? J. Sediment. Petrol. 51 (4), 1147–1156.

Poulet, F. et al., 2005. Phyllosilicates on Mars and implications for early martian climate. Nature 438, 623–627.

Reimers, C.E., Komar, P.D., 1979. Evidence for explosive volcanic density currents on certain martian volcanoes. Icarus 39, 88–110.

Ruesch, O. et al., 2012. Compositional investigation of the proposed chloride-bearing materials on Mars using near-infrared orbital data from OMEGA/MEx. J. Geophys. Res. 117, E00J13.

Sagan, C., Mullen, G., 1972. Earth and Mars: Evolution of atmospheres and surface temperatures. Science 177, 52–56.

Schaber, G.G., 1982. Syrtis major: A low-relief volcanic shield. J. Geophys. Res. 87 (B12), 9852–9866. http://dx.doi.org/10.1029/JB087iB12p09852.

Scott, D.H., Tanaka, K.L., 1986. Geologic Map of the Western Equatorial Region of Mars. United States Geological Survey Miscellaneous Investigations Series, Map I-1802-A, Scale 1:15,000,000.

Seibert, N.M., Kargel, J.S., 2001. Small-scale martian polygonal terrain: Implications for liquid surface water. Geophys. Res. Lett. 28, 899–902.

Smith, P.H. et al., 2009. H$_2$O at the Phoenix landing site. Science 325, 58–61. http://dx.doi.org/10.1126/science.1172339.

Soderblom, L.A. et al., 2004. Soils of Eagle crater and Meridiani Planum at the Opportunity Rover landing site. Science 306, 1723–1726.

Summons, R.E. et al., 2011. Preservation of martian organic and environmental records: Final report of the Mars Biosignature Working Group. Astrobiology 11, 157–184.

Tang, C.-S., Chun Liu, B.S., Suo, W.-B., Gao, L., 2011. Experimental characterization of shrinkage and desiccation cracking in thin clay layer. Appl. Clay Sci. 52, 69–77.

Toramaru, A., Matsumoto, T., 2004. Columnar joint morphology and cooling rate: A starch–water mixture experiment. J. Geophys. Res. 109, B02205. http://dx.doi.org/10.1029/2003JB002686.

Tornabene, L.L., Moersch, J.E., McSween, H.Y., Hamilton, V.E., Piatek, J.L., Christensen, P.R., 2008. Surface and crater-exposed lithologic units of the Isidis Basin as mapped by coanalysis of THEMIS and TES derived data products. J. Geophys. Res. 113, E10.

Vaniman, D.T. et al., 2014. Mineralogy of a mudstone at Yellowknife Bay, Gale crater, Mars. Science 343 (6169). http://dx.doi.org/10.1126/science.1243480.

Velde, B., 2010. Origin and Mineralogy of Clays: Clays and the Environment. Springer-Verlag, Berlin, p. 329.

Viviano, C.E., Moersch, J.E., McSween, A.Y., 2012. Spectral evidence for the carbonation of serpentine in Nili Fossae, Mars. Lunar Planet. Sci. 43. Abstract #2682.

Watters, W.A. et al., 2011. Origin of the structure and planform of small impact craters in fractured targets: Endurance crater at Meridiani Planum, Mars. Icarus 211, 472–497. http://dx.doi.org/10.1016/j.icarus.2010.08.030.

Wendt, L., Bishop, J.L., Neukum, G., 2013. Knob fields in the Terra Cimmeria/Terra Sirenum region of Mars: Stratigraphy, mineralogy and morphology. Icarus 225, 200–215.

Williams, R., Robinson, D., 1989. Origin and distribution of polygonal cracking of rock surfaces. Geogr. Ann. 71A (3–4), 145–159.

Wilson, L., Head, J.W., 2007. Explosive volcanic eruptions on Mars: Tephra and accretionary lapilli formation, dispersal and recognition in the geologic record. J. Volcanol. Geol. Res. 163, 83–97.

Wintzer, A.E., Allen, C.C., Oehler, D.Z., 2011. Phyllosilicate deposits in Shalbatana Vallis. Lunar Planet. Sci. XLII. Abstract #1557.

Wray, J.J., Ehlmann, B.L., Squyres, S.W., Mustard, J.F., Kirk, R.L., 2008. Compositional stratigraphy of clay-bearing layered deposits at Mawrth Vallis, Mars. Geophys. Res. Lett. 35, L12202.

Wray, J.J., Murchie, S.L., Squyres, S.W., Seelos, F.P., Tornabene, L.L., 2009. Diverse aqueous environments on ancient Mars revealed in the southern highlands. Geology 37, 1043–1046.

Wray, J.J., Squyres, S.W., Roach, L.H., Bishop, J.L., Mustard, J.F., Noe Dobrea, E.Z., 2010. Identification of the Ca-sulfate bassanite in Mawrth Vallis, Mars. Icarus 209, 406–421.

Wray, J.J. et al., 2011. Columbus crater and other possible groundwater-fed paleolakes of Terra Sirenum, Mars. J. Geophys. Res. 116, E01001. http://dx.doi.org/10.1029/2010JE003694.

Wray, J.J. et al., 2013. Prolonged magmatic activity on Mars inferred from the detection of felsic rocks. Nat. Geosci.. http://dx.doi.org/10.1038/NGEO1994.